Macromolecules

pubs.acs.org/Macromolecules Article

Stochastic Model of Randomly End-Linked Polymer Network Microregions

Sam C. P. Norris, Andrea M. Kasko, Tom Chou, and Maria R. D'Orsogna*

Cite This: *Macromolecules* 2021, 54, 126–142 Read Online

ACCESS | Metrics & More | Article Recommendations

ABSTRACT: Polymerization and formation of cross-linked polymer networks are important processes in manufacturing, materials fabrication, and in the case of hydrated polymer networks, synthesis of biomedical materials, drug delivery, and tissue engineering. While considerable research has been devoted to the modeling of polymer networks to determine averaged, mean-field, global properties, there are fewer studies that specifically examine the variance of the composition across "microregions" (composed of a large, but finite, number of polymer network strands) within the larger polymer network. Here, we mathematically model the stochastic formation of polymer networks comprised of linear network strands with two identical reactive end-groups that undergo an end-linking gelation process. We focus on networks formed by chain-growth polymerization but also give examples of how our model can be extended to networks formed by step-growth polymerization. We introduce a master equation that describes the evolution of the probabilities of possible network microregion configurations as a function of time and the extent of reaction. We specifically focus on the dynamics of network formation and the statistical variability of the gel microregions, particularly at intermediate extents of reaction. We also consider possible annealing effects and study how cooperative binding between the two end-groups on a single network strand affects network formation. Our results allow for a more detailed and thorough understanding of polymer network dynamics and variability of network properties.

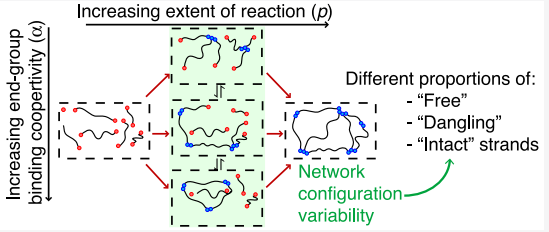

1. INTRODUCTION

The study of cross-linked polymer networks is important in many applications from heavy industry to biomedical research.[1−8] Cross-linked polymer networks can be formed by various techniques, leading to a diverse and complex set of structures and properties. Of these network types, considerable attention has been paid to those formed by a process termed "end-linking." End-linked networks are usually comprised of polymeric precursors, or "network strands," that contain N reactive end-groups.[9,10] During gelation, cross-links, or "branchpoints," link multiple end-groups together. For example, poly(ethylene glycol) (PEG)-based hydrogels, which are common in biomedical applications, are typically formed through the reaction of its end-groups.[11]

Network strands can bind to form a network via two main polymerization reaction mechanisms: chain-growth and step-growth, as shown in Figure 1. Several excellent reviews have been written to describe these processes.[11−14] Briefly, gelation by chain-growth polymerization (Figure 1A) occurs via a chain-extension reaction where the network strand end-groups bind to a growing chain of end-groups, termed the "active center" (e.g., free-radical polymerization of vinyl end-groups). The chain of end-groups forms a branchpoint that cross-links the network strands together. Gelation by step-growth polymerization (Figure 1B) typically involves a defined binary reaction (e.g., thiol−ene or azide−alkyne reactions) between the network strand end-groups and the complementary binding sites of a multifunctional branchpoint, which acts to cross-link the network strands together. In this work, we primarily examine networks formed by chain-growth polymerization but also give examples of how our methods can be applied to step-growth network formation.

Network strands binding via either step- or chain-growth may exist in many states. We examine each end-group in the system and ask if it has bound to a branchpoint or not. Strands in the most representative experimental scenario[9] each carry $N = 2$ reactive groups, one on each end, leading to three possible strand states, as depicted in Figure 1C: (i) the strand may be "free" where neither of the reactive ends have bound (s_0-strand); (ii) the strand may "dangle" where only a single end has bound and the strand dangles from the rest of the network (s_1-strand); or (iii) the strand may be "intact" where both ends are bound to the larger polymer network and bridge two different branchpoints (s_2-strand).[15] Strands with both ends bound may

Received: June 8, 2020
Revised: November 3, 2020
Published: December 30, 2020

https://dx.doi.org/10.1021/acs.macromol.0c01346
Macromolecules 2021, 54, 126−142

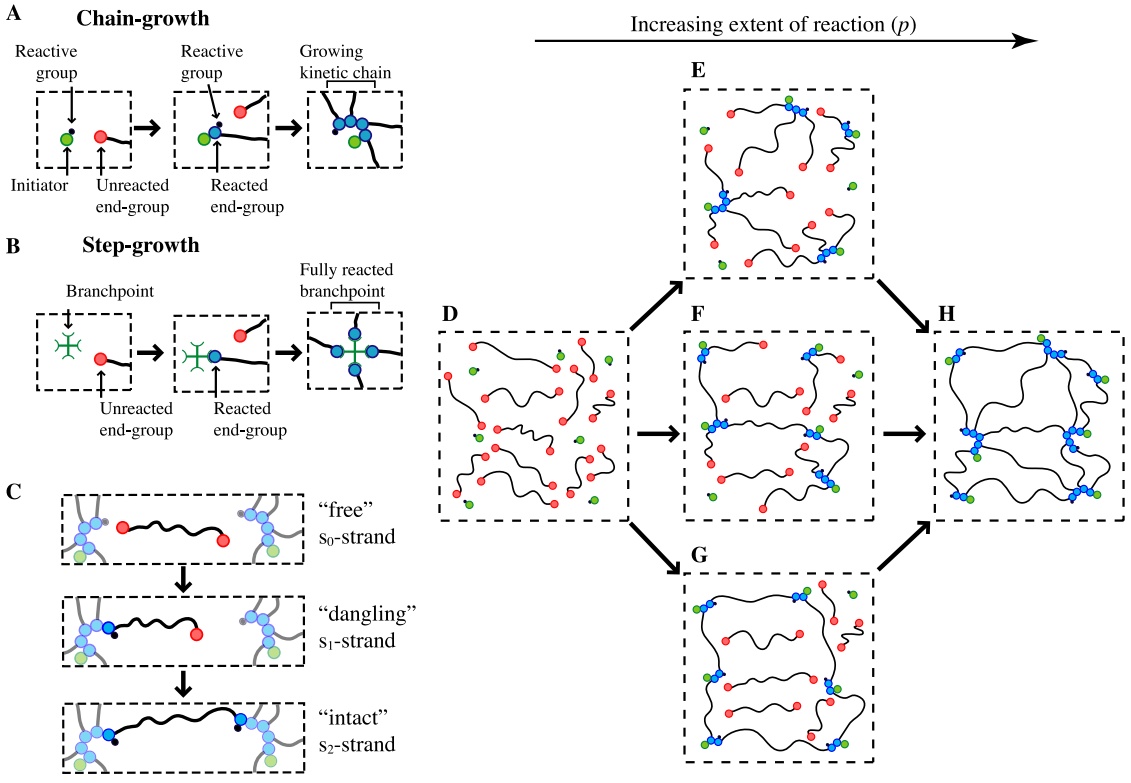

Figure 1. Schematic of the network formation mechanism. (A) In chain-growth polymerization, an initiator reacts with a monomer to produce a propagating species (e.g., radical) that can add to additional chain ends. The reaction terminates after the radical is neutralized or after the occurrence of other terminating reactions. Locally, the reaction center/branchpoint resembles the center of a "star polymer." (B) In step-growth polymerization, network strand end-groups bind to complementary binding sites of a branchpoint with a defined number of functional groups, which cross-link the network strands together. (C−H) Schematic of the local network structure following chain-growth polymerization. Black lines represent network strands with reactive end-groups at each end that can be unbound (red dots) or bound (blue dots). Chain propagation starts at an initiator (green dots) that produces a reactive group (black dot) that propagates down the chain. (C) Strands are either "free"—neither end-group is bound (s_0-strand); "dangling"—a single end-group is bound (s_1-strand); or "intact"—both end-groups are bound (s_2-strand). (D−H) Schematic of five uncoupled "microregions" (dashed lines) within the network. Each is comprised of N_s strands but the extent of reaction p can vary. (D) For $p = 0$, all network strands are in the s_0-state. (E−G) For intermediate $0 < p < 1$, many configurations are possible, including (E) only s_1-strands, (F) a combination of s_0-, s_1-, and s_2-strands, or (G) only s_0- and s_2-strands. (H) For $p = 1$, the only possible microregion configuration is for all the strands be fully bound in the s_2-state.

also form a loop, where both ends are bound to the same branchpoint.[16] The proportion of free, dangling, and intact network strands may affect the chemical and physical properties of the network, for example, in water-swollen polymeric networks, bound strand ratios impact gel modulus, mesh size, and swelling.[3] We assume that further binding at the branchpoint will not affect the state of a given network strand, under both the chain- and step-growth mechanisms. In Section A.1 of the Appendix, we outline the different connective states that lead to free, dangling, and intact states.

Finally, the architecture of polymer networks formed by end-linking gelation is not spatially uniform. Heterogeneous domains within polymer networks exist that span a few to hundreds of nanometers in size and arise through variations in local strand concentration (termed "frozen concentration fluctuation"), heterogeneous distribution of cross-linking, or topological- and connectivity-based inhomogeneities due to variability in network strand assembly.[17−20] We define these microscopic domains as "microregions." For simplicity, we assume that microregions are statistically identical, independent, and composed of a fixed number of N_s strands with two reactive end-groups, resulting in a total of $2N_s$ available binding sites per microregion. We also denote by m the number of bound end-groups in each microregion, so that the fraction p of bound end-groups per microregion is $p = m/(2N_s)$. This quantity is also known as the extent of reaction and can be experimentally tuned to control the elastic modulus, viscosity, swelling, mesh size, and other network properties.[2] By definition $0 \leq p \leq 1$ since the number of bound end-groups m cannot exceed the total number of available ones $2N_s$. Finally, we assume that microregions are large enough that boundary effects between bordering domains are negligible so that the free, dangling, intact strand distribution of two adjacent microregions are not correlated. Note that the same value of $0 < p < 1$ may be associated to different $\{n_0, n_1, n_2\}$ microregion configurations with n_0 free, n_1 dangling, and n_2 intact strands. Figure 1D−H shows five different microregion realizations within a larger network where N_s is fixed but different $\{n_0, n_1, n_2\}$ configurations arise, resulting in different extents of reaction p. In Figure 1E−G, we show several distinct $\{n_0, n_1, n_2\}$ configurations corresponding to fixed N_s and p.

Some quantities of interest may be derived using p such as the likelihood $P_i(p)$[1,2,15,21,22] of finding free ($i = 0$), dangling ($i = 1$), and intact ($i = 2$) strands for a given p. A stochastic analysis however would lead to an expression for the probability distribution of finding any microregion configuration $\{n_0, n_1, n_2\}$ corresponding to a given p, offering a much richer understanding of the binding process. Previously developed stochastic models use a subset-of-states approach,[23−25] where a

https://dx.doi.org/10.1021/acs.macromol.0c01346
Macromolecules 2021, 54, 126−142

polymerizing mixture is described as a set of "subgraph" states of monomeric strands, a subset of which is used to drive polymerization.[26,27] These models, however, only examine the connectivity of small subgraphs, typically made of only a few network strands, to represent large-scale networks and predict bulk quantities such as the network gel point.[26,28] Studies involving larger subgraphs containing a sizable number of strands (say, greater than 10) are still lacking. Finally, although several Monte Carlo numerical studies have examined network heterogeneity,[29−35] none of them have evaluated configuration probability distributions.

We aim to determine the probability distribution for a given configuration of free, dangling, and intact strands within a microregion of N_s strands with two reactive end-groups, for fixed m bound end-groups, or equivalently for fixed $p = m/2N_s$. This will allow us to go beyond the characterization of a microregion by means of p and N_s alone and to obtain analytical expressions for microregion properties that depend on possible $\{n_0, n_1, n_2\}$ configurations. In some experimental scenarios, m or p may change among microregion realizations, and it may be useful to understand the structure of the network for a given average, intermediate extent of reaction $\langle p \rangle$. Our results will thus be presented both as a function of time and of the average extent of reaction. We draw on existing stochastic self-assembly and nucleation models[36−40] and utilize a master equation approach. Different forms of the master equation will be developed and analyzed to account for different end-group reactivities and the possibility for end-groups to dynamically rearrange within the microregion. In Figure 1E−G, when $0 < p < 1$, a single $\{n_0, n_1, n_2\}$ state could be representative of a large number of possible network topologies and connectivities. For simplicity, we do not model branchpoint functionality, nor the formation of loops or other complex topological structures, leaving the inclusion of such features to future studies. In this work, we only focus on the number of intact, dangling, and free $\{n_0, n_1, n_2\}$ strands within microregions; as a result, the total number of branchpoints and topology of the network do not affect our modeling. Table 1 lists the various quantities used in the remainder of this work.

2. MATHEMATICAL MODELS AND ANALYSIS

For completeness, we first review basic combinatoric methods used to study equilibrium network configurations. We then introduce a master equation to describe quenched end-group binding in chain-growth polymerization. The master equation we formulate allows end-groups to dynamically detach and reattach and use it as a model for reversible network polymerization. A variation of this master equation that can be applied to step-growth polymerization is presented in Section A.4 of the Appendix.

Table 1. Summary of Variables Used

symbol	representation
N	number of reactive end-groups per network strand
i	number of bound end-groups per network strand
s_i	designation of strand type with i bound end-groups
N_s	number of network strands per microregion
n_0	number of s_0-network strands per microregion
n_1	number of s_1-network strands per microregion
n_2	number of s_2-network strands per microregion
m	total number of bound end-groups per microregion
p	extent of reaction, $p = m/(N_sN)$
t	time of reaction (time units)
$P(n_1, n_2, t)$	microregion configuration $\{n_0, n_1, n_2\}$ probability at t
α	end-group-binding cooperativity (unitless)
λ	binding rate (time^{-1})
κ	end-group rearrangement rate to binding rate ratio (unitless)

2.1. Combinatoric Methods. Many mathematical studies of network formation via end-linking have used combinatoric approaches to quantify the number of polymeric strands in a given state.[15,41−44] The extent of reaction p, defined as the fraction of bound end-groups per microregion, can also be interpreted as the probability that any end-group within a microregion has bound. The probability $P_i(p)$ of finding an s_i-strand with $0 \le i \le N$ bound end-groups is thus

$$P_i(p) = \binom{N}{i} p^i (1-p)^{N-i} \tag{1}$$

which assumes that of N end-groups, i are bound and $N - i$ are not. Equation 1 provides a basis for mean-field end-linking gelation models used to predict network properties. Henceforth, we assume $N = 2$. The average number $n_i(p)$ of s_i strands within a microregion of N_s strands can thus be written as

$$n_i(p) = N_s \binom{2}{i} p^i (1-p)^{2-i} \tag{2}$$

2.1.1. Limitations of the Combinatoric Approach. The binding scenarios illustrated in Figure 1D−H reveal that many possible configurations exist for a given microregion. Evaluating the probability that any of them may arise requires a more complex mathematical representation than eqs 1 or 2, which do not provide any information on the possible distribution of free, dangling, and intact strands within a microregion. Furthermore, the combinatoric approach outlined above yields mean-field, equilibrated determinations of network strand composition and does not allow for specific/alternate network formation processes to be studied. These include quenched end-group binding, the presence of specific reaction steps, or network strand binding cooperativity, which we address below.

Quenched end-group binding. The reaction steps associated with network formation may be irreversible or reversible. Irreversible reactions lead to the formation of "quenched" networks whose properties are highly dependent on initial conditions. This nuance cannot be captured by eq 2, which implies equilibration and is independent of initial conditions. Reversible reactions instead allow the network to rearrange while forming, and "anneal," yielding configurations that are independent of initial conditions. As we shall see, equilibrated and averaged quantities in the absence of cooperativity may be described by eq 2.

Reaction steps during polymerization. End-group binding proceeds via a specific sequence of steps under chain-growth polymerization, as detailed in Figure 1A. In chain growth, when a propagating species binds with an unreacted end-group, the propagating species is no longer active but is replaced by a new propagating end-group, allowing further end-group binding to the chain. End-group binding to an active center (or "branchpoint") occurs sequentially, and at any given time only one reactive site exists at the active center/branchpoint. Thus, when end-groups line up in a chain (Figure 1A), the strand ends may be attached to two other end-groups and the network strands might be considered "tetrafunctional," according to common polymer chemistry terminology. For example, Flory modeled the formation of networks formed by tetrafunctional

https://dx.doi.org/10.1021/acs.macromol.0c01346
Macromolecules 2021, 54, 126−142

divinyl compounds using mean-field theory.[45] While the use of the "tetrafunctional strand" nomenclature might seem reasonable, it can be misleading in the context of quenched end-group binding during chain polymerization. While each strand end has two potential binding sites, the end-group must first bind to an active center before further binding to that end-group can occur. Combinatorial models of tetrafunctional network strands do not capture this nuance. Thus, each end is best described as a single reactive site that can ultimately bind a variable number of other strand ends to form a branchpoint (Figure 1A) until the reactive site is terminated; each strand is assumed to have a total of two reactive ends ($N = 2$). Moreover, this work does not keep track of the size of the branchpoints (length of the kinetic chains) but only studies the state of the network strands within a microregion. We leave the enumeration of branchpoints to future studies where the problem can be mapped onto one of heterogeneous nucleation.[39]

Binding cooperativity. Some end-groups may also bind differently than others depending on their intramolecular state, a process we call "binding cooperativity" or "binding uncooperativity" depending on whether binding is favored or hindered, respectively. In the mathematical models we present below, cooperative effects will be embodied by the parameter α, representing the overall effect of different forces that cause certain binding events to occur with higher or less likelihood than others. Specifically, $\alpha > 1$ represents cooperative binding so that $s_1 \rightarrow s_2$ binding events are more likely than $s_0 \rightarrow s_1$ events. The reverse is true for uncooperative binding; when $\alpha < 1$ $s_0 \rightarrow s_1$ events are favored. Cooperative or uncooperative intramolecular network strand end-group binding effects may have several chemical and/or physical origins. Cooperative binding may arise when the unbound end-group of a dangling strand more readily binds to form a fully bound, intact strand due to its proximity to the polymerizing network, especially when the polymer solution is dilute.[28] Cooperative binding may also occur if binding of s_0 free strands is inhibited. For example, dense polymer solutions may restrict the movement of free strands to find an appropriate binding site.

Uncooperative binding emerges when s_2 strand formation from the binding of an existing s_1 strand is hindered by negative allosteric effects, which has been shown to occur, for example, in rigid strands.[35] Uncooperative binding also emerges when s_1 strand formation from the binding of an s_0 strand is enhanced. For example, free strands might more readily bind than dangling ones since diffusion allows them to more easily navigate the local environment to find an appropriate reaction site. Hence, dangling strands form more readily than intact ones.

Binding cooperativity may also be dependent on the time or extent of reaction. For example, network strand diffusion coefficients change as the network becomes more fully formed, which could restrict the binding of free strands. In addition, at higher extents of reaction, if a strand is bound at one end to a branchpoint, the other end could bind to another branchpoint only if the branchpoints (and the strands emanating from them) do not exclude each other. The shielding of the branchpoints might then prevent a dangling strand from efficiently finding another branchpoint to attach to. Similarly, if the network strands are long, binding of free strands to a crowded branchpoint may be prevented. Crowding will be dependent on the goodness of the solvent as well as on the configurations of the branchpoints (which we do not consider here). While we do not examine such effects in this work, they can be modeled by setting α to be a function of various network properties: $\alpha(N_s, n_2, n_1, ...)$.

2.2. Stochastic Model of Chain-Growth Polymerization: The Master Equation for Quenched End-Group Binding. We now derive the probability distribution $P(n_0, n_1, n_2, t)$ of finding a given $\{n_0, n_1, n_2, t\}$ microregion configuration at time t through a master equation that allows for the inclusion of reversible/irreversible (annealed/quenched) bond formation and cooperative/uncooperative binding. Note that two major assumptions applied in this work are well-mixing and independence: each strand within a given microregion can bind independently of its position within the microregion itself, and strands do not interact with one another. We neglect spatial arrangements of network strands and the branchpoints that they bind to; this assumption could limit our approach if the microregions are very large and end-groups do not have access to every available binding site within the microregion. Since the total number of strands per microregion is constant, the constraint $n_0 + n_1 + n_2 = N_s$ is obeyed at all times and effectively $P(n_0, n_1, n_2, t) \rightarrow P(n_1, n_2, t)$. We compare equilibrium or steady-state solutions to eq 1; where possible, we also determine the full time-dependent solution for $P(n_1, n_2, t)$, which can be used to derive other quantities of interest, such as the variance and higher moments. We first consider the case of irreversible (or quenched) end-group binding, whereby once an end-group has bound, it will not detach. In chain-growth polymerizations, the binding rate λ of an end-group will depend on the number of available reactive sites (radicals, anions, cations, etc.), which exist either as active initiators or as active sites of the growing polymer chain. The number of available reactive sites may also change in time or depend on the extent of reaction. For example, autoacceleration can occur as the network structure forms, decreasing localized diffusion speeds, and hence the speed at which termination occurs. Similarly, if active initiator formation is slow or termination events occur before all end-groups are bound, λ will more strongly depend on the time and extent of reaction.

For simplicity, we assume that the number of available reactive sites is constant and that active site termination does not occur (which is the case for living polymerizations[46]). Thus, the binding rate λ of an end-group will be a constant and does not depend on the extent of reaction. Conversely, when constructing master equation models of step-growth polymerization, which we briefly explore in Section A.4 of the Appendix, one must consider that the number of complementary binding sites decreases as the extent of reaction increases.

Future extensions of this work can include more complex kinetics where λ depends on the extent of reaction and the specific microregion configuration: $\lambda(N_s, n_2, n_1, ...)$ or by adding a specific prefactor to the master equation as we demonstrate in Section A.4 of the Appendix. Under these conditions, the master equation for the probability distribution $P(n_1, n_2, t)$ evolves according to

$$\begin{aligned}\frac{dP(n_1, n_2, t)}{dt} &= 2\lambda(N_s - n_1 - n_2 + 1)P(n_1 - 1, n_2, t) \\ &\quad + \lambda\alpha(n_1 + 1)P(n_1 + 1, n_2 - 1, t) \\ &\quad - \lambda[2(N_s - n_1 - n_2) + \alpha n_1]P(n_1, n_2, t)\end{aligned} \tag{3}$$

where we have explicitly used the $n_0 = N_s - n_1 - n_2$ constraint. Equation 3 also includes the reactivity parameter α, as described

https://dx.doi.org/10.1021/acs.macromol.0c01346
Macromolecules 2021, 54, 126−142

in Section 2.1.1: $\alpha > 1$ represents cooperative binding so that $s_1 \rightarrow s_2$ binding events are more likely than $s_0 \rightarrow s_1$ events; the reverse is true for uncooperative binding, $\alpha < 1$, where $s_0 \rightarrow s_1$ events are favored. The first term on the right-hand side of eq 3 represents the process of an unbound strand attaching to the network structure to form a singly bound dangling strand ($s_0 \rightarrow s_1$), which gives the configuration transition $\{n_0 + 1, n_1 - 1, n_2\} \rightarrow \{n_0, n_1, n_2\}$ (Figure 2). The multiplicative factor $N_s - n_1 - n_2 + 1$ represents the number s_0 strands in the starting configuration that can bind to the network; the 2 prefactor is included since an s_0 strand can bind to the network at either of its two unbound end-groups. Similarly, the second term represents an unbound end-group from a singly bound strand binding to the network and forming a doubly bound strand ($s_1 \rightarrow s_2$). The related transition is $\{n_0, n_1 + 1, n_2 - 1\} \rightarrow \{n_0, n_1, n_2\}$ (Figure 2). The multiplicative factor $n_1 + 1$ represents the number of s_1 strands that can bind to the network to form an s_2 strand. Finally, the last term describes the processes that drive the system out of the $\{n_0, n_1, n_2\}$ configuration, where either an $s_0 \rightarrow s_1$ transition, with $\{n_0, n_1, n_2\} \rightarrow \{n_0 - 1, n_1 + 1, n_2\}$, or an $s_1 \rightarrow s_2$ transition, with $\{n_0, n_1, n_2\} \rightarrow \{n_0, n_1 - 1, n_2 + 1\}$, occur (Figure 2). The total number of distinct $\{n_0, n_1, n_2\}$ states can be enumerated via

$$\sum_{n_2=0}^{N_s} \sum_{n_1=0}^{N_s-n_2} 1 = \frac{(N_s + 2)(N_s + 1)}{2} \tag{4}$$

Due to the irreversibility of the binding process, at $t \rightarrow \infty$ we expect the system to consist only of s_2-network strands: $P(n_1, n_2, t \rightarrow \infty) = 0$ for all $\{n_1, n_2\} \neq \{0, N_s\}$ and $P(0, N_s, t \rightarrow \infty) = 1$, as depicted in Figure 1H. We can obtain an alternate representation for eq 3 using the $n_0 + n_1 + n_2 = N_s$ constraint to represent n_2 so that $P(n_0, n_1, n_2, t) \rightarrow P(n_0, n_1, t)$ and the master equation reads

$$\begin{aligned} \frac{dP(n_0, n_1, t)}{dt} &= 2\lambda(n_0 + 1)P(n_0 + 1, n_1 - 1, t) \\ &\quad + \lambda\alpha(n_1 + 1)P(n_0, n_1 + 1, t) \\ &\quad - \lambda(2n_0 + \alpha n_1)P(n_0, n_1, t) \end{aligned} \tag{5}$$

This representation is equivalent to eq 3 and will be useful in deriving the distribution $P(n_0, n_1, t)$ from which $P(n_1, n_2, t)$ can be obtained. We now nondimensionalize our model by measuring time in units of the typical bond formation time, λ^{-1}. Henceforth, time t will be dimensionless and λ will no longer appear (equivalently, we set $\lambda = 1$ in eqs 3 and 5). The mean number of strand types $\langle n_i(t)\rangle$ in single microregions are defined by

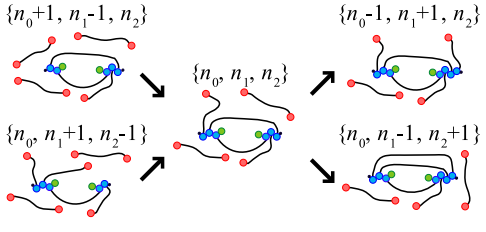

Figure 2. Possible end-group binding transitions for $N_s = 6$. The state at the center of the schematic is $\{n_0, n_1, n_2\} = \{2, 2, 2\}$ corresponding to $m = 6$. To the left are two $m = 5$ and to the right are two $m = 7$ configurations. Under quenched binding discussed in Section 2.2, the dynamics will flow from left to right following the unidirectional arrows.

$$\langle n_i(t)\rangle = \sum_{n_1,n_2} n_i P(n_1, n_2, t) \tag{6}$$

for $i = 1, 2$, under the $0 \leq n_1 + n_2 \leq N_s$ constraint. The corresponding mass-action equations can be derived by multiplying eq 3 by n_i and by summing over n_1, n_2 under the same constraint so that

$$\frac{d\langle n_0(t)\rangle}{dt} = -2\langle n_0\rangle \tag{7a}$$

$$\frac{d\langle n_1(t)\rangle}{dt} = 2\langle n_0\rangle - \alpha\langle n_1\rangle \tag{7b}$$

$$\frac{d\langle n_2(t)\rangle}{dt} = \alpha\langle n_1\rangle \tag{7c}$$

Equations 7a–7c can be solved under the initial condition $n_0(0) = N_s$, representing all strands being unbound at $t = 0$. We find

$$\langle n_0(t)\rangle = N_s\, e^{-2t} \tag{8a}$$

$$\langle n_1(t)\rangle = N_s \frac{2(e^{-\alpha t} - e^{-2t})}{2 - \alpha} \tag{8b}$$

$$\langle n_2(t)\rangle = N_s\left(1 + \frac{\alpha\, e^{-2t} - 2\, e^{-\alpha t}}{2 - \alpha}\right) \tag{8c}$$

so that $\langle n_i(t\rightarrow\infty)\rangle \rightarrow 0$ for $i = 0$, 1 and $\langle n_2\,(t \rightarrow \infty)\rangle \rightarrow N_s$. Equations 8a–8c represent average values calculated across all microregions at time t under quenched binding. We compare eqs 8a–8c to eq 2, which estimates average strand numbers using combinatoric arguments. To do so, we evaluate $\langle m\rangle = \langle n_1\rangle + 2\,\langle n_2\rangle$ to find

$$\langle m(t)\rangle = \frac{2N_s}{2 - \alpha}[2 - \alpha - e^{-\alpha t} + (\alpha - 1)\, e^{-2t}] \tag{9}$$

from which we calculate the average extent of reaction $\langle p(t)\rangle = \langle m(t)\rangle/2N_s$

$$\langle p(t)\rangle = 1 - \frac{1}{2 - \alpha}[e^{-\alpha t} - (\alpha - 1)\, e^{-2t}] \tag{10}$$

Inverting the transcendental eqs 9 and 10 for general α is not possible; however, under neutral cooperativity $\alpha = 1$, we find

$$\langle p(t)\rangle = 1 - e^{-t} \tag{11}$$

A simple analysis of eqs 10 and 11 reveals that $\langle p(t)\rangle$ is a monotonically increasing function of t for all $\alpha > 0$, which is expected given that end-groups bind but do not unbind. For $\alpha = 1$, eqs 8a–8c can be recast as

$$\langle n_0\rangle = N_s(1 - \langle p\rangle) \tag{12a}$$

$$\langle n_1\rangle = 2N_s\langle p\rangle(1 - \langle p\rangle) \tag{12b}$$

$$\langle n_2\rangle = N_s\langle p\rangle^2 \tag{12c}$$

Equations 12a–c have the same form as eq 2, obtained using mean-field arguments. This implies that the mean-field approach for a given extent of reaction p and $\alpha = 1$ corresponds to an irreversible (quenched) stochastic process halted at time t^* such that $\langle p(t^*)\rangle$ in eq 11 satisfies $\langle p(t^*)\rangle = 1 - e^{-t^*} = p$. We plot the normalized average strand numbers $\langle n_i(t)\rangle/N_s$ as a function of time and as derived from eqs 8a–8c in Figure 3A–C, for $N_s = 40$ and different values of α. We find that s_1 strand formation is

https://dx.doi.org/10.1021/acs.macromol.0c01346
Macromolecules 2021, 54, 126–142

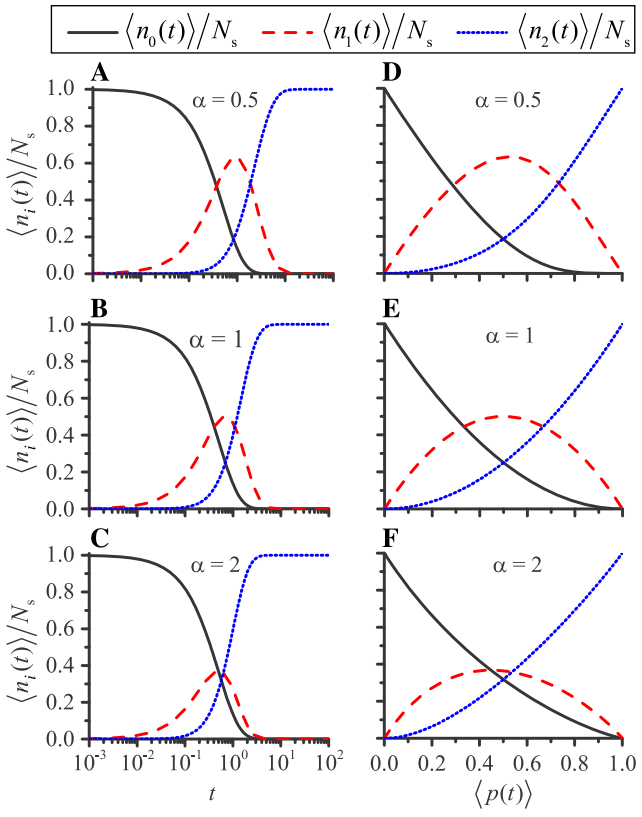

Figure 3. Average strand fractions $\langle n_i(t)\rangle/N_s$ for i = 0, 1, 2 and N_s = 40 as evaluated from eqs 8a−8c and plotted as a function of (A−C) time and (D−F) parametrically against the extent of reaction $\langle p(t)\rangle$ given by eq 10. The chosen values of the reactivity parameter α are: (A, D) α = 0.5, (B, E) α = 1, and (C, F) α = 2.

favored at smaller α, and s_2 strand formation is favored at higher α, as might be expected. Since $\langle p(t)\rangle$ is a monotonic function of time, we can plot $\langle n_i(t)\rangle/N_s$ using eqs 8a−8c as parametric equations against $\langle p(t)\rangle$ given in eq 10. Results are shown in Figure 3D−F for various values of α. These curves differ from those derived from the solution to the mean-field eq 2. Most noticeably, $\langle n_1(t)\rangle$ loses its symmetry about $\langle p(t)\rangle$ = 0.5 and becomes skewed.

The master eq 3 also allows us to derive the time-dependent likelihood of each of the many possible configurations (enumerated in eq 4), a much more powerful tool than average quantities. For example, eq 3 can be solved to find $P(n_1, n_2, t)$ for all times t once the initial condition is specified. We set this to be $P(n_1 = 0, n_2 = 0, t = 0) = 1$ and $P(n_1, n_2, t = 0) = 0$ for all other values of $n_1, n_2 \neq 0$, so that the microregion is initially made only of free strands. If one chooses to solve eq 5 to find $P(n_0, n_1, t)$ the equivalent initial conditions are $P(n_0 = N_s, n_1 = 0, t = 0) = 1$ and $P(n_0, n_1, t = 0) = 0$ for $n_0 \neq N_s$ and $n_1 \neq 0$. We solve eq 5 for $P(n_0, n_1, t)$ rather than eq 3 for $P(n_1, n_2, t)$ as the analytical computations are simpler. From $P(n_0, n_1, t)$, we can then derive $P(n_1, n_2, t)$ by changing variables through the $n_0 + n_1 + n_2 = N_s$ constraint. To proceed, we introduce the generating function $G(z_0, z_1, t)$ defined as

$$G(z_0, z_1, t) = \sum_{n_0, n_1} P(n_0, n_1, t) z_0^{n_0} z_1^{n_1} \tag{13}$$

under the constraint $0 \leq n_0 + n_1 \leq N_s$. Upon multiplying eq 5 by $z_0^{n_0} z_1^{n_1}$ and summing over n_0, n_1, under the same constraint, we find the following differential equation for $G(z_0, z_1, t)$

$$\frac{\partial G}{\partial t} = 2(z_1 - z_0)\frac{\partial G}{\partial z_0} + \alpha(1 - z_1)\frac{\partial G}{\partial z_1} \tag{14}$$

Equation 14 is coupled to the corresponding initial condition $G(z_0, z_1, t = 0) = z_0^{N_s}$. Using the method of characteristics, we find

$$G(z_0, z_1, t) = \left[z_0\, e^{-2t} + \frac{2z_1(e^{-\alpha t} - e^{-2t})}{2 - \alpha} + 1 + \frac{\alpha\, e^{-2t} - 2\, e^{-\alpha t}}{2 - \alpha} \right]^{N_s} \tag{15}$$

After performing a Taylor series expansion in z_0,z_1 and upon comparison with eq 13, we find

$$P(n_0, n_1, t) = \binom{N_s}{n_0, n_1} e^{-2tn_0} \left(\frac{2(e^{-\alpha t} - e^{-2t})}{2 - \alpha} \right)^{n_1} \times \left(1 + \frac{\alpha\, e^{-2t} - 2\, e^{-\alpha t}}{2 - \alpha} \right)^{N_s - n_0 - n_1} \tag{16}$$

From the constraint $n_0 = N_s - n_1 - n_2$, we can finally write

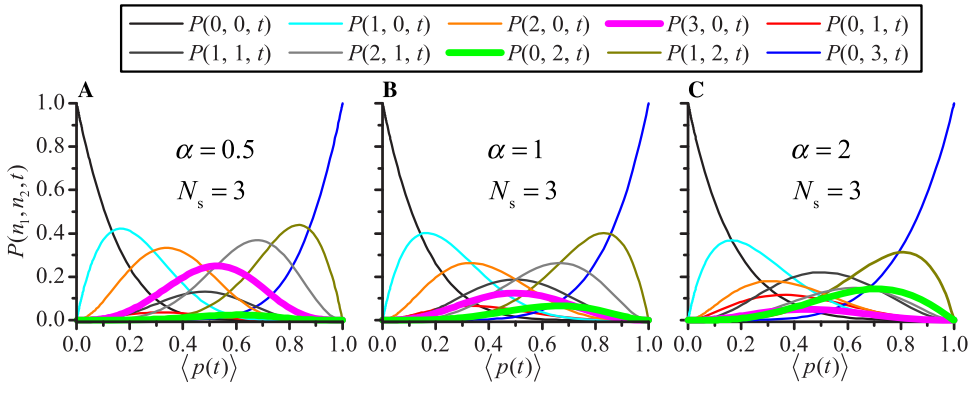

Figure 4. Probability distributions $P(n_1, n_2, t)$ for N_s = 3 under quenched binding, as evaluated from eq 17. We plot $P(n_1, n_2, t)$ parametrically against $\langle p(t)\rangle$, as evaluated from eq 10 for (A) α = 0.5, (B) α = 1, and (C) α = 2. Of the 10 possible configurations, two are highlighted: $\{n_0, n_1, n_2\} = \{0, 3, 0\}$ (magenta) and $\{1, 0, 2\}$ (green).

https://dx.doi.org/10.1021/acs.macromol.0c01346
Macromolecules 2021, 54, 126−142

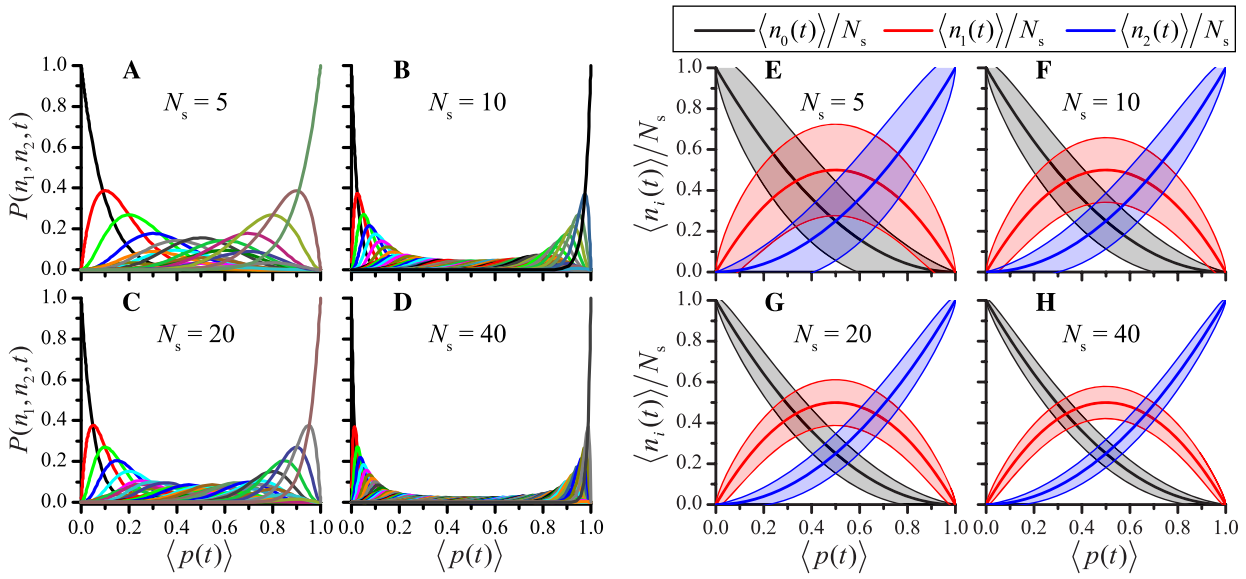

Figure 5. (A–D) Probability distributions $P(n_1, n_2, t)$ for several values of N_s under quenched binding, as evaluated from eq 17. We set $\alpha = 1$ and plot $P(n_1, n_2, t)$ parametrically against $\langle p(t) \rangle$, as evaluated from eq 10. (E–H) Average strand fractions $\langle n_i(t) \rangle / N_s$ for $i = 0, 1, 2$ plotted parametrically against $\langle p(t) \rangle$. Standard deviations are calculated as the square root of the variance in eq 21a; shaded areas represent the associated error intervals. Chosen N_s values are (A, E) $N_s = 5$, (B, F) $N_s = 10$, (C, G) $N_s = 20$, and (D, H) $N_s = 40$.

$$P(n_1, n_2, t) = \binom{N_s}{n_1, n_2} e^{-2t(N_s - n_1 - n_2)} \left(\frac{2(e^{-\alpha t} - e^{-2t})}{2 - \alpha} \right)^{n_1} \times \left(1 + \frac{\alpha e^{-2t} - 2 e^{-\alpha t}}{2 - \alpha} \right)^{n_2} \tag{17}$$

Note that $P(n_1, n_2, t \to \infty) = 0$ for $\{n_1, n_2\} \neq \{0, N_s\}$ and that $P(0, N_s, t \to \infty) = 1$ as expected from a forward process. Figure 4 shows the probability of individual configurations $P(n_1, n_2, t)$ of microregions with $N_s = 3$ plotted parametrically against $\langle p(t) \rangle$ for different values of α. Two different configurations are highlighted: $\{n_0, n_1, n_2\} = \{0, 3, 0\}$ and $\{1, 0, 2\}$. For $\alpha = 2$, when end-group binding is cooperative, the probability of configurations with more s_1 strands decreases and those with more s_2 strands increases compared to the neutral ($\alpha = 1$) or uncooperative ($\alpha = 0.5$) cases shown here. In highly cooperative scenarios, once a network strand has bound the transition toward a fully bound s_2-strand is fast. In Figure 5A–D, we plot the microregion configuration probabilities $P(n_1, n_2, t)$ as a function of the average extent of reaction $\langle p(t) \rangle$ with increasing N_s. The highest value of $N_s = 40$ we used results in 861 distinct $\{n_0, n_1, n_2\}$ microregion configurations, as per eq 4, all with nonzero probability at a finite time. Larger values of N_s are possible but graphically difficult to display.

By inserting the explicit expression for $P(n_1, n_2, t)$ from eq 17 into eq 6, we evaluate the average values $\langle n_i(t) \rangle$ for $i = 1, 2$ to reobtain the same expressions for $\langle n_i(t) \rangle$, for $i = 0, 1, 2$ already displayed in eqs 8a–8c. From eq 17, we can also calculate the second moments $\langle n_i^2(t) \rangle$ as

$$\langle n_i^2(t) \rangle = \sum_{n_1, n_2} n_i^2 P(n_1, n_2, t) \tag{18}$$

for $i = 1, 2$, and the correlation function

$$\langle n_1(t) n_2(t) \rangle = \sum_{n_1, n_2} n_1 n_2 P(n_1, n_2, t) \tag{19}$$

from which we can derive $\langle m^2(t) \rangle$

$$\langle m^2(t) \rangle = \sum_{n_1, n_2} (n_1 + 2n_2)^2 P(n_1, n_2, t) = \langle n_1^2(t) \rangle + 4\langle n_2^2(t) \rangle + 4\langle n_1(t) n_2(t) \rangle \tag{20}$$

Using eqs 8a–8c, 9, 18, and 19 we find the variances

$$\mathrm{Var}(n_i(t)) = \langle n_i^2(t) \rangle - \langle n_i(t) \rangle^2, \tag{21a}$$

$$\mathrm{Var}(m(t)) = \langle m^2(t) \rangle - \langle m(t) \rangle^2 \tag{21b}$$

for $i = 1, 2$. Finally, $\langle n_0^2 \rangle$ is obtained as

$$\langle n_0^2(t) \rangle = \sum_{n_1, n_2} (N_s - n_1 - n_2)^2 P(n_1, n_2, t) = N_s^2 + \langle n_1^2(t) \rangle + \langle n_2^2(t) \rangle + N_s \langle n_1(t) \rangle + N_s \langle n_2(t) \rangle + \langle n_1(t) n_2(t) \rangle \tag{22}$$

Equations 22 and 8a–8c yield $\mathrm{Var}(n_0(t)) = \langle n_0^2(t) \rangle - \langle n_0(t) \rangle^2$. Explicit expressions for $\langle n_i^2(t) \rangle$, $\langle m^2(t) \rangle$, $\mathrm{Var}(n_i(t))$, and $\mathrm{Var}(m(t))$ are presented in Section A.2 of the Appendix. In Figure 5E–H, we show the parametric plots of the average strand fractions $\langle n_i(t) \rangle / N_s$ for $i = 0, 1, 2$ against the average extent of reaction $\langle p(t) \rangle$ for several values of N_s. The associated standard deviations calculated as the square root of the variance in eq 21a are also displayed. As can be expected, fluctuations decrease as N_s increases. Figure 6A shows the parametric plot of $\mathrm{Var}(n_2(t))$ against $\langle p(t) \rangle$ for different values of α and $N_s = 40$. For strong uncooperative binding ($\alpha \to 0$) and small extents of reaction $\langle p(t) \rangle$, only free strands bind to the network and the variance is very small. However, once all strands have bound at least at one end, and $\langle p(t) \rangle \sim 0.5$, the dangling strands transition to the fully bound state and the variance starts increasing. In eq 33 of Section A.2 of the Appendix, we give an exact analytical expression for $\mathrm{Var}(n_2(t))$; a simple calculation shows that the maximum variance is $N_s/4$ for all values of α and is attained at smaller average extents of reaction $\langle p(t) \rangle$ as α increases. In

https://dx.doi.org/10.1021/acs.macromol.0c01346
Macromolecules 2021, 54, 126–142

Figure 6B, we plot the parametric dependence of $\mathrm{Var}(p(t))$ against the average extent of reaction $\langle p(t)\rangle$ with variable α and $N_s = 40$. For very small values of $\alpha \to 0$, $\mathrm{Var}(p(t))$ is bimodal and approximately zero at $\langle p(t)\rangle \to 0.5$. This is because, as discussed above, for $\alpha \to 0$ end-group binding occurs only on free strands for $\langle p(t)\rangle < 0.5$ and the most likely configurations are those with s_0 and s_1 strands. As $\langle p(t)\rangle \to 0.5$, only s_1 dangling strands remain so that $\langle n_1(t)\rangle \to N_s$, $\langle {n_1}^2(t)\rangle \to N_s^2$, and $\mathrm{Var}(n_2(t)) \to 0$, and as a result, $\mathrm{Var}(p(t)) \to 0$. Fully bound strands start emerging for $\langle p(t)\rangle > 0.5$, increasing $\mathrm{Var}(p(t))$. As α increases, the variance increases for all $\langle p(t)\rangle$ and the minimum at $\langle p(t)\rangle \sim 0.5$ turns into a maximum. A more detailed discussion is presented in Section A.3 of the Appendix.

In Figure 6C, we plot $\mathrm{Var}(n_2(t))/{N_s}^2$ against $\langle p(t)\rangle$ for different values of N_s; the curves decrease in magnitude as N_s increases. Finally, in Figure 6D we plot $\langle n_1(t)\rangle/N_s$ parametrically against $\langle p(t)\rangle$ for several values of α. The curves decrease with α once $\langle p(t)\rangle$ is fixed. This also follows from eq 8b, which implies that $\langle n_1(t)\rangle$ is a decreasing function of α for any time t. Since $\langle p(t)\rangle$ is univocally associated to t via eq 10, it also follows that $\langle n_1(t)\rangle$ is a decreasing function of α for any $\langle p(t)\rangle$. Equations 8b and 10 reveal that the maximum $\langle n_1(t_{max})\rangle/N_s = (\alpha/2)^{(1-2/\alpha)}$ is attained at $\langle p(t_{max})\rangle = 1 - ((\alpha + 1)/\alpha)\, e^{-2t_{max}}$ where $t_{max} = \ln(2/\alpha)/(2 - \alpha)$. One can easily verify that $\langle p(t_{max})\rangle$ is a decreasing function of α as well. These results can be expected as larger α favors the formation of fully bound strands. Thus, for a given average extent of reaction $\langle p(t)\rangle$, the fraction of dangling ends decreases with α and the maximum is found at an average extent of reaction $\langle p(t)\rangle$ that also decreases with α.

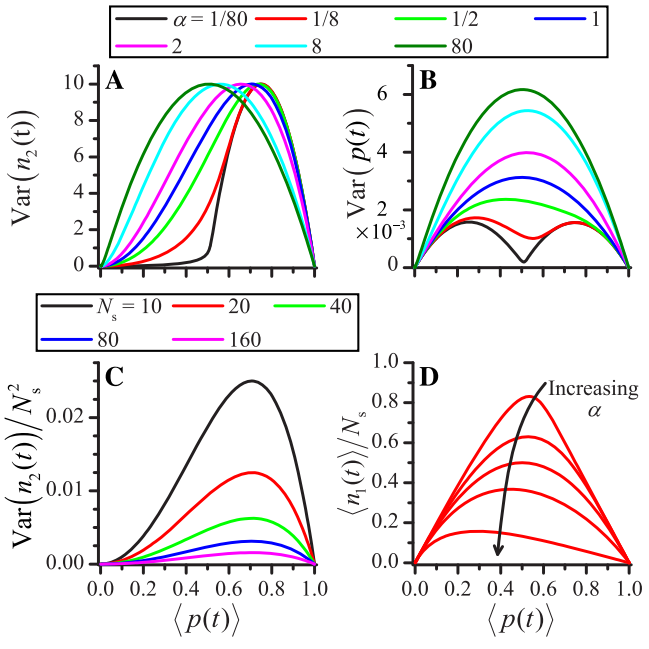

Figure 6. Variance of the number of (A) s_2 strands and of (B) extent of reaction p, as evaluated by eq 21a for $\alpha = 1/8$, 1/2, 1, 2, or 8 and $N_s = 40$. $\mathrm{Var}(n_2(t))$ and $\mathrm{Var}(p(t))$ are plotted parametrically against $\langle p(t)\rangle$, as evaluated from eq 10. For $\alpha > 80$ and $\alpha < 1/80$, the curves do not change significantly from those displayed. (C) Variance of the fraction of s_2 strands $\mathrm{Var}(n_2)/N_s^2$ for $N_s = 10$, 20, 40, 80, and 160 and $\alpha = 1$. (D) Relative $\langle n_1(t)\rangle/N_s$, as calculated from eq 8b for $\alpha = 1/8$, 1/2, 1, 2, or 8 and $N_s = 40$.

2.3. Dynamic End-Group Rearrangement/Redistribution. We now consider an equilibration process that allows the bound end-groups in a microregion to dynamically rearrange, attaching and detaching until thermodynamic equilibrium is reached[47] while maintaining a fixed total number of m bound end-groups. We assume that $m < 2N_s$, $(p < 1)$ so that the reaction is not complete and multiple $\{n_0, n_1, n_2\}$ configurations are possible. Experimental realizations include the formation reversible hydrazone bonds,[48] imine bonds,[49] guest−host interactions,[50] among many other mechanisms.[51] While most polymer networks that include dynamic bonds are typically made of network strands with more than two reactive end-groups, dynamic allyl sulfide bonds have recently been introduced into network strands with only two end-groups that cross-link via multifunctional branchpoints.[52] We can thus envision the possibility of introducing other types of dynamic covalent bonds into network strands with two reactive end-groups as well.[51] We also note that bond rearrangement may be less realistic for networks formed by chain-growth polymerization (compared to networks formed by step-growth polymerization, which we briefly explore in Section A.4 of the Appendix). However, one could construct a network strand with reversible covalent bonds at its end-groups terminated by a moiety that can undergo chain polymerization, such as an acrylate. While not the same type of dynamic covalent chemistry described here, network strands that polymerize into photodegradable hydrogels are constructed in this manner.[53] Finally, we use bond rearrangement to directly compare the results of eq 3 to mean-field theory (eq 2) and combinatorial models (Section A.5 of the Appendix) that assume binding and unbinding occur until equilibrium has been reached; we demonstrate that such models are not accurate representations of networks formed by quenched end-group binding.

During the rearrangement process, an intact s_2 strand may detach at one of its ends to form a dangling s_1 strand, while a free s_0 strand binds to the network to form another s_1 strand (Figure 7). The reverse process where two s_1 strands become an s_2 and s_0 strand is also possible. In all scenarios $m = n_1 + 2n_2$ is fixed, but there are many distinct ways for the bound end-groups to distribute in s_1 or s_2 strands. The final equilibrium configuration is independent of initial conditions so our results will depend only on the selected value of m. We write the reversible master equation for $P(n_1, n_2, t)$ as

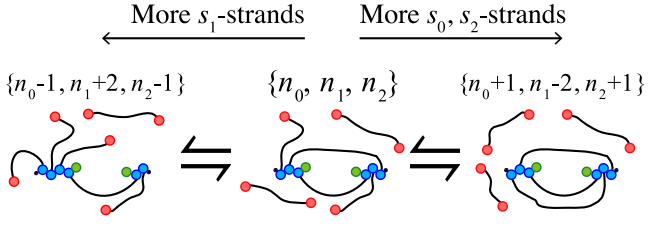

Figure 7. Possible end-group bond rearrangement transitions for $N_s = 6$. The state at the center is $\{n_0, n_1, n_2\} = \{2, 2, 2\}$ corresponding to $m = 6$, $p = 0.5$. From right to left, the number of dangling s_1 strands increases, from left to right, the number of intact s_2 and free s_0 strands increase, Throughout, $m = 6$ remains fixed. Dynamic rearrangement, as discussed in Section 2.3, allows strands to equilibrate among $\{n_0, n_1, n_2\}$ states with the same m, similarly to the three shown here for $m = 6$.

https://dx.doi.org/10.1021/acs.macromol.0c01346
Macromolecules 2021, 54, 126−142

$$\frac{dP(n_1, n_2, t)}{dt} = 2\kappa\alpha^2 \binom{n_1 + 2}{2} P(n_1 + 2, n_2 - 1, t)$$
$$+4\kappa(N_s - n_1 - n_2 + 1)(n_2 + 1)P(n_1 - 2, n_2 + 1, t)$$
$$-2\kappa\alpha^2 \binom{n_1}{2} P(n_1, n_2, t)$$
$$-4\kappa n_2(N_s - n_1 - n_2)P(n_1, n_2, t) \quad (23)$$

Here, κ is dimensionless and represents the rearrangement rate measured in terms of the binding rate. The first term on the right-hand side of eq 23 accounts for the formation of a fully bound s_2 strand and a free s_0 strand from two dangling s_1 strands ($2s_1 \rightarrow s_0 + s_2$). Here, the bound end-group of one of the two s_1 strands exchanges with the unbound end-group of the other, leading to the $\{n_0 - 1, n_1 + 2, n_2 - 1\} \rightarrow \{n_0, n_1, n_2\}$ transition, as shown in Figure 7. The combinatorial factor enumerates the number of s_1 strands present in the microregion and the 2 prefactor represents both s_1 strands being able to exchange with the other. Finally, the reactivity parameter α is squared, since two dangling ends must bind to form a fully bound strand. The second term represents a fully bound s_2 strand detaching on one end while promoting the binding of a free s_0 strand, giving rise to two dangling s_1 strands. This process is represented by the $\{n_0 + 1, n_1 - 2, n_2 + 1\} \rightarrow \{n_0, n_1, n_2\}$ transition, as shown in Figure 7. The factors $(N_s - n_1 - n_2 + 1)$ and $(n_2 + 1)$ represent the number of s_0 and s_2 network strands available, respectively. The prefactor 4 accounts for the number of possible bond movements: either of the two bound end-groups on the s_2 strand can relocate to either of the two unbound end-groups of the s_0-strand, yielding a total of four combinations. The last two terms represent the same two processes described above but driving the system away from $\{n_0, n_1, n_2\}$. Note that there are no terms in eq 23 representing bonds leaving an s_2 strand to populate an s_1 strand; this transition would not change the overall the microregion configuration $\{n_0, n_1, n_2\}$. The probability $P_b(m,t)$ of having m bound-ends at time t can be written as

$$P_b(m, t) = \sum_{n_2=0}^{[m/2]} P(m - 2n_2, n_2, t) \quad (24)$$

where all possible n_1, n_2 combinations that yield $m = n_1 + 2n_2$ are included. Using eq 23, it can be easily verified that $P_b(m,t) = P_b(m,t = 0)$. As expected, the master eq 23 only rearranges the distribution of s_1 and s_2 strands, but m remains unchanged. We thus assume that the system is initiated with a given m so that $n_1 + 2n_2 = m$ at all times. In addition to this constraint, the number of strands is fixed so that $n_0 + n_1 + n_2 = N_s$. We can thus cast eq 23 in terms of only one of the n_0, n_1, or n_2 populations. We choose n_2 and determine the steady-state $P(n_1, n_2, t \rightarrow \infty) \equiv P^*(n_2)$ by imposing a detailed balance between the first and the last terms on the right-hand side of eq 23 or equivalently the second and the third, since it can be easily verified that the conditions are the same. We find

$$\frac{P^*(n_2 - 1)}{P^*(n_2)} = \frac{4n_2(N_s - m + n_2)}{\alpha^2(m - 2n_2 + 2)(m - 2n_2 + 1)} \quad (25)$$

which can be solved to yield

$$P^*(n_2) = \frac{1}{Z_{m,N_s}} \frac{(2/\alpha)^{m-2n_2} N_s!}{(m - 2n_2)!n_2!(N_s - m + n_2)!} \quad (26)$$

where Z_{m,N_s} is the normalization constant

$$Z_{m,N_s} = \sum_{n_2=0}^{[m/2]} \frac{(2/\alpha)^{m-2n_2} N_s!}{(m - 2n_2)!n_2!(N_s - m + n_2)!} \quad (27)$$

This result is the same as eq 56 of Section A.5 of the Appendix when a combinatorial approach is taken to approximate microregion configuration probabilities for a fixed m; this approach is equivalent to allowing for relaxation on the network with a fixed number of bound-ends and $m = 2pN_s$.

2.3.1. End-Group Rearrangement/Redistribution and Bond Formation. We now consider the two processes of bond formation and redistribution occurring simultaneously and combine the two master eqs 3 and 26 so that

$$\frac{dP(n_1, n_2, t)}{dt} = 2(N_s - n_1 - n_2 + 1)P(n_1 - 1, n_2, t)$$
$$+\alpha(n_1 + 1)P(n_1 + 1, n_2 - 1, t)$$
$$+\kappa\alpha^2(n_1 + 2)(n_1 + 1)P(n_1 + 2, n_2 - 1, t)$$
$$+4\kappa(N_s - n_1 - n_2 + 1)(n_2 + 1)P(n_1 - 2, n_2 + 1, t)$$
$$-[\kappa\alpha^2 n_1(n_1 - 1) + 4\kappa n_2(N_s - n_1 - n_2)$$
$$+2(N_s - n_1 - n_2) + \alpha n_1]P(n_1, n_2, t) \quad (28)$$

Fast annealing, fast binding, and quenched/irreversible binding are modeled by setting $\kappa \gg 1$, $\kappa \ll 1$, and $\kappa = 0$, respectively. Although a full analytical time-dependent solution cannot be found, the effects of annealing can be observed in Figure 8. Here, we parametrically plot $P(n_1, n_2, t)$ against $\langle p(t) \rangle$ using eq 28 for $N_s = m = 5$, $\alpha = 0.5$, and $\alpha = 2$, under fast annealing ($\kappa = 1000$) or quenched binding ($\kappa = 0$). Since the rearrangement process allows for more configurations to be explored, we expect cooperative effects to be more pronounced under fast annealing than under quenched binding. In Figure 8A, we set $\alpha = 0.5$; since binding is uncooperative, annealing favors configurations with lower values of n_2. Indeed, the $k = 1000$ curves show an increase in $P(5, 0, t)$ compared to the corresponding $\kappa = 0$ curves, whereas $P(3, 1, t)$, $P(1, 2, t)$ decrease. Similar trends are observed in Figure 8B, where we set $\alpha = 2$. Cooperative binding

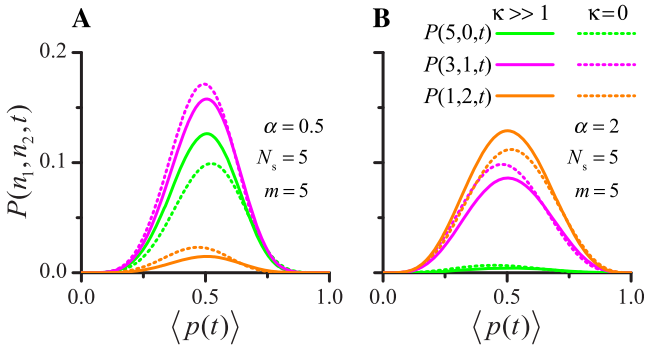

Figure 8. Configuration probabilities $P(n_1, n_2, t)$ calculated from eq 28 and plotted parametrically against $\langle p(t) \rangle$ under fast annealing ($\kappa = 1000$, solid lines) and quenched binding ($\kappa = 0$, dashed lines) for $N_s = 5$ and (A) $\alpha = 0.5$, $m = 5$; (B) $\alpha = 2$, $m = 5$.

https://dx.doi.org/10.1021/acs.macromol.0c01346
Macromolecules 2021, 54, 126−142

increases the likelihood of configurations with higher n_2, so in this case, $P(1, 2, t)$ increases, while $P(3, 1, t)$, $P(5, 0, t)$ decrease. Note that $P(5, 0, t)$, $P(3, 1, t)$, and $P(1, 2, t)$ all obey the constraint $n_1 + 2n_2 = N_s = 5$. For $\alpha = 2$, and under quenched binding at $\kappa = 0$, eq 17 yields $P(5, 0, t) = 32\, e^{-10t} t^5$, which is maximized at $t = 1/2$ corresponding to $\langle p(t = 1/2)\rangle = 1 - 3/2\, e \neq 1/2$, as per eq 10. Similarly, $P(3, 1, t) = 8\, e^{-8t} t^3(1 - (2t + 1)\, e^{-2t})$ and $P(1, 2, t) = 2\, e^{-6t} t(1 - (2t + 1)\, e^{-2t})$ are also maximized at times that correspond to $\langle p(t)\rangle \neq 1/2$. None of the three distribution curves are thus symmetric about $\langle p(t)\rangle = 1/2$. When $\kappa = 1000$, however the master eq 28 yields numerical results that are closely aligned with those derived from eq 23 upon setting $n_1 + 2n_2 = N_s = 5$. This is because annealing is much faster than binding and the time between binding events is much longer than the time for equilibration of a fixed number of bound strands. As a result, once a strand binds, the network can almost fully equilibrate before the next binding event occurs. The curves in Figure 8B for $\kappa = 1000$ thus mirror eq 26, with the proportions $P(5, 0)$:$P(3, 1)$:$P(1, 2)$ following eq 25 and become symmetric about $\langle p(t)\rangle = 0.5$, as predicted by eq 26 when $m = N_s$. The same trends arise when comparing the quenched binding and the fast annealing curves for the uncooperative ($\alpha = 0.5$) case.

In Figure 9, we plot $\langle n_i(t)\rangle/N_s$ parametrically against $\langle p(t)\rangle$ for $\alpha = 0.5$, 1, and 2 using the probability distribution in eq 28 for $i = 0$, 1, 2 and $\kappa = 1000$. The most notable feature is the symmetry of $\langle n_1(t)\rangle$ about $\langle p(t)\rangle = 0.5$ for all α, a feature of the combinatoric approach, as discussed in Section A.5 of the Appendix. Intermediate values of $\kappa \approx 1$ yield curves that interpolate between the two extremes $\kappa \gg 1$ and $\kappa = 0$ shown here. Our results imply that networks formed via quenched end-group binding, as per eq 17, should not be described by models that assume network strands equilibration via redistribution, as per eq 1 and eq 57 in Section A.5 of the Appendix.

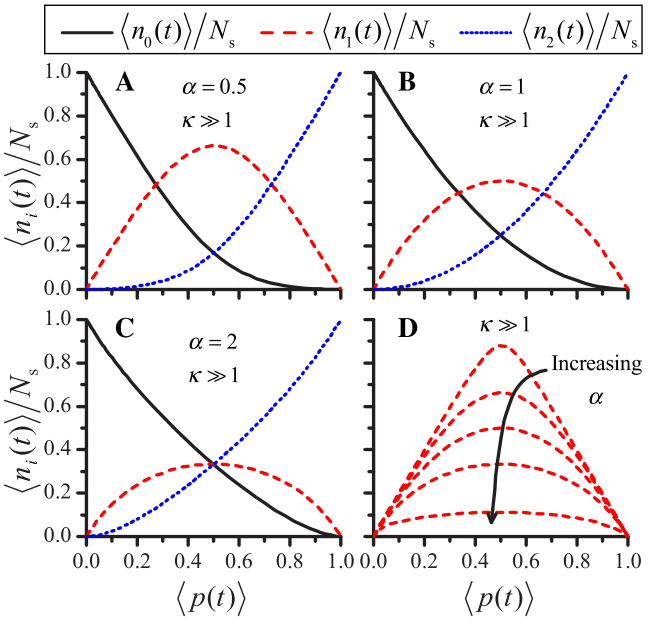

Figure 9. Average strand fractions $\langle n_i(t)\rangle/N_s$ for $i = 0$, 1, 2 and $N_s = 10$ evaluated using the probability distribution in eq 28 and plotted parametrically against $\langle p(t)\rangle$ under fast annealing ($\kappa = 1000$). The reactivity parameter is set as (A) $\alpha = 0.5$, (B) $\alpha = 1$, and (C) $\alpha = 2$. All curves closely resemble those obtained from the equilibrium distribution in eq 26. (D) Under fast annealing, $\langle n_1(t)\rangle/N_s$ is symmetric about $\langle p(t)\rangle = 0.5$ for all α, here set at $\alpha = 1/8$, 1/2, 1, 2, and 8, from top to bottom.

3. DISCUSSION AND CONCLUSIONS

In this work, we studied the stochastic properties of network strands with two reactive ends that undergo an end-linking gelation process. We developed and analyzed a master equation to describe quenched and annealed binding events in micro-regions within a larger polymer network and include a reactivity parameter to model cooperative effects. While typical models quantify "average" mean-field properties, we are able to evaluate the full probability distribution for any given configuration as a function of time and the extent of reaction. By modeling the probability of a configuration within a microregion, we can propose a crude framework to describe the effects of heterogeneity across the entire sample.

For example, our approach can be used in several polymer network applications under the assumption that a macroscopic region is comprised of a collection of statistically identical, independent, smaller microregions (Figure 10). For example, nano/micrometer-scale differences in the polymer network properties can affect the fate of cells that are cultured on them[54] as well as the mechanical properties of high-performance materials.[55] If these properties depend on the local number of free, dangling, and intact strands, we can use the relevant probability distribution to evaluate the likelihood of a given configuration $\{n_0, n_1, n_2\}$ in any number of microregions sampled by, e.g., a cell. The statistical distribution for each microregion can then be used to construct the probability distribution of the entire macrosystem and thus to estimate the chemical or mechanical properties of the polymer network, including their local variability.

Similar considerations can be applied to the study of elastic properties, in particular within the phantom network theory, which posits that the shear modulus of an ideal network depends on the number density of elastically effective network strands. While complex topological features that affect network mechanical properties (including primary loops,[17] which we do not tabulate here) can form, our results are readily applicable if we assume that s_2 strands are elastically effective and the number of branchpoints is fixed. Starting from the probability $P(n_1, n_2, t)$ that a microregion is in the $\{n_0, n_1, n_2\}$ configuration,

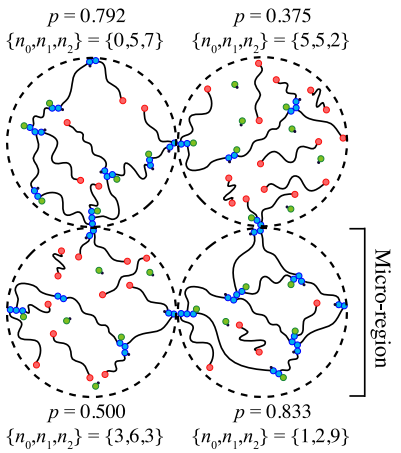

Figure 10. Schematic of four uncoupled "microregions" (dashed lines) within the network. Each is comprised of N_s strands but the extent of reaction p can vary.

https://dx.doi.org/10.1021/acs.macromol.0c01346
Macromolecules 2021, 54, 126−142

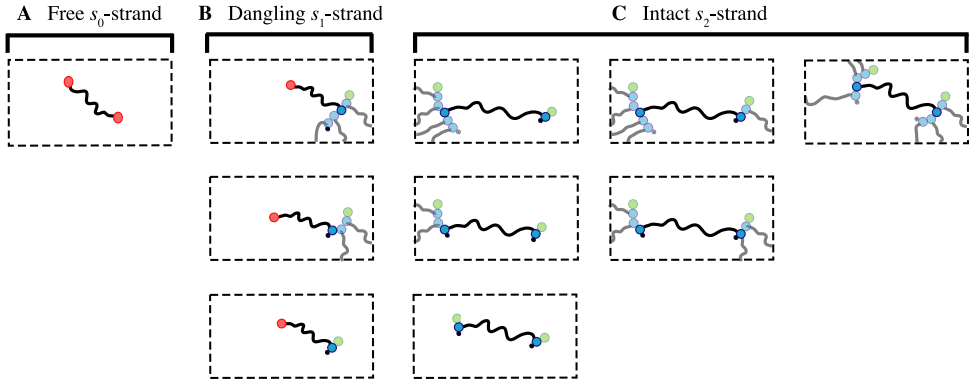

Figure 11. Different scenarios of network strand attachment to the network. (A) For a free s_0 strand, neither end-group is bound. (B) For a dangling s_1 strand, one end-group is unbound, and the other can be connected to either the middle of a polymerizing chain, at the end of the chain at the reactive site, or to a chain that only consists of an initiator and the bound end-group of interest. (C) Intact s_2 strand consists of two end-groups bound to a chain. Similarly, each bound end-group may independently exist in the middle of the kinetically growing chain, at the reactive site of the chain, or to a chain that only consists of an initiator.

we can also compute the likelihood that a given threshold is met, say, $n_2 \geq n_2^*$. This quantity can then be interpreted as the probability for a "bond" to stretch across a microregion. One can then calculate the likelihood that a given number of contiguous microregions with $n_2 \geq n_2^*$ span the sample through percolation, leading to a dramatic stiffening of the network. In future iterations of this model, branchpoint functionality can be examined using models of heterogeneous nucleation,[39] and models of network theory can be incorporated to determine the probability of different cyclic defects such as finite-strand aggregates, loops, and other topologies,[27] all of which may affect the mechanical properties of the network.

Finally, our work can also be applied to the study of network degradation, which has attracted much attention over the past two decades as degradable sites have been increasingly incorporated into experimental realizations of end-linking polymerization. These degradable strands typically cleave by enzymatic, hydrolytic, photolytic, or other chemical mechanisms and allow for a reverse gelation process. Here, strands initially exist in the fully bound, intact state where both ends are unreacted. Reverse gelation occurs via reaction or degradation of either end, so that intact strands first become dangling strands, and dangling strands then become free strands. Halting the extent of reaction is common in degradable networks as a way to tune the gel mechanics and this results in a large variability of the microregion composition. Photodegradable networks formed by the end-linking of network strands with two end-groups that can be degraded by exposure to light[44,53,56−65] are of particular interest as they are uniquely suited to spatially pattern network stiffness, with a high degree of control.[66] Some mathematical models of reverse gelation have been formulated by adapting models of gelation;[15] more specific mean-field photodegradable network models have also been proposed.[43,44] The present work can be adapted to model degradable networks by associating intact network strands to s_0 strands (zero degraded end-groups), dangling strands to s_1 strands (one degraded end-group), and free strands to s_2 strands (two degraded end-groups). Cooperative effects arise in this context as the undegraded end-groups of an intact strand might more readily react due to tension across the strand induced by network swelling. Once one of the end-groups has cleaved and the strand dangles, the stress is removed so that the remaining undegraded end-group is less susceptible to further degradation. Using our stochastic framework, one can calculate the probability of any given microregion configuration, distinguishing between quenched and annealed network degelation reactions. Melting and collapse of rigidity can then be described using percolation concepts.

APPENDIX

A.1. Connectivity of a Network Strand

During network formation, a strand with $N = 2$ reactive end-groups may exist in one of three states: (i) the two end-groups are unbound and the strand is free (s_0 strand); one end-group is bound and the other is not, so the strand "dangles" from the network (s_1 strand); and finally, both end-groups are bound to a branchpoint or to a polymerizing chain and the strand is intact (s_2 strand). During end-group binding, the size of the polymerizing chain and the position of the bound end-group along the chain may differ (see Figure 11). The end-group may be attached only to an initiator, within the chain, or at the reactive site, at the end. For simplicity, we define a single end-group bound to an initiator as a branchpoint. Each scenario, however, does not change the inherent state of the network strand of interest (free, dangling, intact). In our definition, each end-group is either unbound or bound. We then count the number of corresponding s_0, s_1, and s_2 strands, regardless of the state of the branchpoint to which each end-group is attached.

A.2. Second Moments

We here derive $\langle n_i^2(t)\rangle$, $\mathrm{Var}(n_i(t))$, and $\mathrm{Var}(m(t))$ for $i = 0, 1, 2$ using the explicit form for $P(n_1, n_2, t)$, as given in eq 17. We begin with

$$\langle n_i^2(t)\rangle = \sum_{n_2=0}^{N_s} \sum_{n_1=0}^{N_s-n_2} n_i^2 P(n_1, n_2, t) \tag{29}$$

and the associated variances for $i = 1, 2$. Using the binomial theorem, we find

$$\langle n_1^2(t)\rangle = \frac{2N_s}{(2-\alpha)^2}(e^{-\alpha t} - e^{-2t}) \times [2 - \alpha + 2(N_s - 1)(e^{-\alpha t} - e^{-2t})] \tag{30}$$

which coupled with eq 8b for $\langle n_1(t)\rangle$ leads to

https://dx.doi.org/10.1021/acs.macromol.0c01346
Macromolecules 2021, 54, 126−142

$$\mathrm{Var}(n_1(t)) = \frac{2N_s}{(2-\alpha)^2}(e^{-\alpha t} - e^{-2t}) \times (2 - \alpha - 2\,e^{-\alpha t} + 2\,e^{-2t}) \quad (31)$$

Similarly, eq 29 for $i = 2$ yields

$$\langle n_2^2(t)\rangle = \frac{N_s}{(2-\alpha)^2}(2 - \alpha - 2\,e^{-\alpha t} + \alpha\,e^{-2t}) \times [N_s(2 - \alpha - 2\,e^{-\alpha t} + \alpha\,e^{-2t}) + 2\,e^{-\alpha t} - \alpha\,e^{-2t}] \quad (32)$$

which, coupled with eq 8c for $\langle n_2(t)\rangle$, leads to

$$\mathrm{Var}(n_2(t)) = \frac{N_s}{(2-\alpha)^2}(2 - \alpha - 2\,e^{-\alpha t} + \alpha\,e^{-2t}) \times (2\,e^{-\alpha t} - \alpha\,e^{-2t}) \quad (33)$$

Equation 33 is maximized for time t_M implicitly given by

$$2\,e^{-\alpha t_M} - \alpha\,e^{-2t_M} = \frac{2-\alpha}{2} \quad (34)$$

which corresponds to $\mathrm{Var}(n_2(t_M)) = N_s/4$, independent of the value of α. To evaluate $\langle m^2(t)\rangle$, we must first calculate the correlation function

$$\langle n_1(t)n_2(t)\rangle = \sum_{n_2=0}^{N_s}\sum_{n_1=0}^{N_s-n_2} n_1 n_2 P(n_1, n_2, t) \quad (35)$$

which yields

$$\langle n_1(t)n_2(t)\rangle = \frac{2N_s(N_s-1)}{(2-\alpha)^2}(e^{-\alpha t} - e^{-2t}) \times (2 - \alpha - 2\,e^{-\alpha t} + \alpha\,e^{-2t}) \quad (36)$$

We can now evaluate $\langle m^2(t)\rangle$ using eqs 20, 30, and 32

$$\langle m^2(t)\rangle = \frac{4N_s^2}{(2-\alpha)^2}[2 - \alpha + (\alpha-1)e^{-2t} - e^{-\alpha t}]^2 + \frac{2N_s}{(2-\alpha)^2}[(2-\alpha)(e^{-\alpha t} + (3-2\alpha)\,e^{-2t}) - 2[(\alpha-1)\,e^{-2t} - e^{-\alpha t}]^2] \quad (37)$$

from which the variance is obtained as

$$\mathrm{Var}(m(t)) = \frac{2N_s}{(2-\alpha)^2}[(2-\alpha)(e^{-\alpha t} + (3-2\alpha)\,e^{-2t}) - 2[(\alpha-1)\,e^{-2t} - e^{-\alpha t}]^2] \quad (38)$$

where we used eqs 8b and 8c to evaluate $\langle m(t)\rangle$. Finally, using the constraint $n_0 = N_s - n_1 - n_2$, we find

$$\langle n_0^2(t)\rangle = N_s[N_s\,e^{-4t} + e^{-2t}(1 - e^{-2t})] \quad (39)$$

which together with eq 8a finally yields

$$\mathrm{Var}(n_0(t)) = N_s\,e^{-2t}(1 - e^{-2t}) \quad (40)$$

A.3. Strong Uncooperative Binding

All evaluations in the main text assume $\alpha \neq 0$, since the completely uncooperative case ($\alpha = 0$) would not allow for the formation of s_2 strands. Setting $\alpha = 0$ however can be used to explore the short time behavior when $\alpha \to 0$. This is the case of highly uncooperative binding where although rare, the formation of a fully bound s_2 strand is still possible. Setting $\alpha = 0$ in eqs 8b, 8c, and 10, so that $e^{-\alpha t} \to 1$ for all times, we find

$$\langle n_1(t)\rangle = N_s(1 - e^{-2t}) \quad (41)$$

$$\langle n_2(t)\rangle = 0 \quad (42)$$

$$\langle p(t)\rangle = \frac{1}{2}(1 - e^{-2t}) \quad (43)$$

Upon setting $\alpha = 0$ in eq 38, we also find

$$\mathrm{Var}(p(t)) = \frac{1}{4N_s^2}\mathrm{Var}(m(t)) = \frac{1}{4N_s}e^{-2t}(1 - e^{-2t}) = \frac{1}{4N_s}2\langle p(t)\rangle(1 - 2\langle p(t)\rangle) \quad (44)$$

Note that eq 43 yields $\langle p(t)\rangle < 0.5$ for all times, implying that for $\alpha = 0$ the reaction cannot be completed, as expected since fully bound strands cannot emerge. Equation 44 also reveals that $\mathrm{Var}(p(t))$ is symmetric about $\langle p\rangle = 1/4$ and its maximum is attained at $\mathrm{Var}(p(t)) = (16N_s)^{-1}$. The above results still apply in the $\alpha \to 0$ limit, albeit for $\alpha t \ll 1$ where $e^{-\alpha t} \to 1$. For example, $\mathrm{Var}(p(t))$ follows eq 44 in Figure 6B up to $\langle p(t)\rangle \sim 0.5$. At longer times, since α is small but not zero, the binding will proceed, and s_2 strands will emerge. We can thus re-evaluate eqs 8b, 8c, and 10, for $\alpha \to 0$ but at long times where $e^{-2t} \to 0$ and $e^{-\alpha t} \neq 0$ so that

$$\langle n_1(t)\rangle = N_s\,e^{-\alpha t} \quad (45)$$

$$\langle n_2(t)\rangle = N_s(1 - e^{-\alpha t}) \quad (46)$$

$$\langle p(t)\rangle = 1 - \frac{1}{2}e^{-\alpha t} \quad (47)$$

Finally, in the $e^{-2t} \to 0$ limit, eq 38 becomes

$$\mathrm{Var}(p(t)) = \frac{1}{4N_s^2}\mathrm{Var}(m(t)) = \frac{1}{4N_s}e^{-\alpha t}(1 - e^{-\alpha t}) = \frac{1}{4N_s}2\langle p(t)\rangle(1 - 2\langle p(t)\rangle) \quad (48)$$

The results in eqs 47 and 48 indicate that as $t \to \infty$, $\langle p(t)\rangle > 0.5$ and $\langle p(t)\rangle \to 1$. Furthermore, we observe that the shape of $\mathrm{Var}(p(t))$ in eq 48 is the same as in eq 44 as also emerges from the bimodal form in Figure 6B. Finally, we note that for $t \to \infty$, $\langle n_1(t)\rangle \to 0$, even as $\alpha \to 0$ since eventually all strands will be fully bound and $\langle n_2(t)\rangle \to N_s$.

A.4. Stochastic Model of Step-Growth Polymerization Using the Master Equation

In Section 2.2, we presented a master equation to model the probability of different network strand configurations within a microregion. Equation 3 is specific to networks formed by chain-growth polymerization. Modifications are necessary to make it applicable to networks formed by step-growth polymerization. Thus, in Figure 12 we show the possible end-group binding transitions during step-growth polymerization of $N = 2$ network strands, which are the equivalent of Figures 2 and 7 for chain-growth polymerization. Step-growth polymerization reactions only involve binding between an end-group and an open,

https://dx.doi.org/10.1021/acs.macromol.0c01346
Macromolecules 2021, 54, 126−142

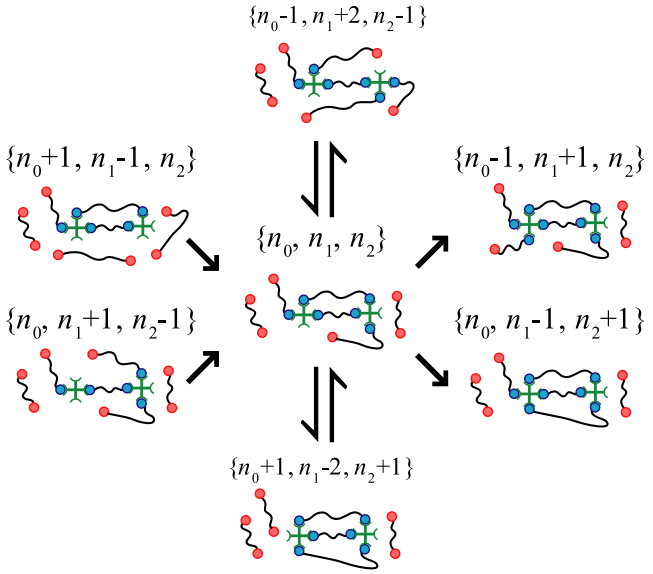

Figure 12. Possible end-group binding transitions during step-growth polymerization for $N_s = 6$. The state at the center of the schematic is $\{n_0, n_1, n_2\} = \{2, 2, 2\}$ corresponds to $m = 6$. To the left are two $m = 5$ and to the right are two $m = 7$ configurations. Under quenched binding, the dynamics will flow from left to right following the unidirectional arrows. To the top and bottom of the $\{n_0, n_1, n_2\} = \{2, 2, 2\}$ state are other $m = 6$ configurations. Under dynamic rearrangement, the system equilibrates following the vertical lines.

complementary binding site on a multifunctional branchpoint. Multistep binding as in chain-growth polymerization does not occur. Additionally, the functionality of the branchpoint is usually defined in step-growth. Thus, the probability distribution $P(n_1, n_2, t)$ for step-growth can be written as

$$\begin{aligned}\frac{dP(n_1, n_2, t)}{dt} &= 2\lambda(2N_s - n_1 - 2n_2 + 1) \\ &\quad \times (N_s - n_1 - n_2 + 1)P(n_1 - 1, n_2, t) \\ &+ \lambda\alpha(2N_s - n_1 - 2n_2 + 1)(n_1 + 1)P(n_1 + 1, n_2 - 1, t) \\ &- \lambda(2N_s - n_1 - 2n_2)[2(N_s - n_1 - n_2) + \alpha n_1]P(n_1, n_2, t)\end{aligned} \tag{49}$$

As can be seen by comparing eq 49 with eq 3, there is an extra prefactor in each term. These represent the number of complementary binding sites, which is given by the total number of end-groups $2N_s$ in each microregion, minus the number of end-groups that have already bound, given by the number of s_1 strands and twice the number of s_2 strands, since they are engaged in two end-group bindings. For example, the factor $2N_s - n_1 - 2n_2 + 1$ is exactly the number of open, available binding sites in a microregion with $n_1 - 1$ single strands and with n_2 intact strands, given by $2N_s - (n_1 - 1) - 2n_2$. Similar reasoning applies to all additional factors in eq 49 that do not appear in eq 3. We leave the analysis of eq 49 to future work. Here, we end by examining step-growth network formation when bonds are allowed to reversibly bind and rearrange within the network. As shown in Figure 12, bond rearrangements can occur by which the unbound end-group of an s_1 strand binds to the network to become an s_2 strand; at the same time, a different s_1 strand unbinds from the network to become an s_0 strand. The reverse process is also possible by which an s_0 and s_2 strand become two s_1 strands. Under step-growth polymerization, these rearrangement events are more realistic than under chain-growth polymerization (Table 2). Indeed, it has been recently demonstrated that reversible covalent bonds can be used to generate a multitude of step-growth networks.[51]

Conveniently, the redistribution dynamics are independent of whether bond formation occurs via step or chain growth, implying that eq 23 is applicable to both polymerization processes. This is because of the fundamental assumption that the rearrangement of bonds between two strands occurs in a pair-wise fashion without the need for other auxiliary strands to mediate the process and thus without the need to enumerate them. For step-growth polymerization, if we allow both bond formation and redistribution to occur simultaneously we can combine the two master eqs 23 and 49 so that

$$\begin{aligned}\frac{dP(n_1, n_2, t)}{dt} &= 2\lambda(N_s - n_1 - 2n_2 + 1) \\ &\quad \times (N_s - n_1 - n_2 + 1)P(n_1 - 1, n_2, t) \\ &+ \lambda\alpha(N_s - n_1 - 2n_2 + 1)(n_1 + 1)P(n_1 + 1, n_2 - 1, t) \\ &+ \kappa\alpha^2(n_1 + 2)(n_1 + 1)P(n_1 + 2, n_2 - 1, t) \\ &+ 4\kappa(N_s - n_1 - n_2 + 1)(n_2 + 1)P(n_1 - 2, n_2 + 1, t) \\ &- \lambda(N_s - n_1 - 2n_2)[2(N_s - n_1 - n_2) + \alpha n_1]P(n_1, n_2, t) \\ &- \kappa\alpha^2 n_1(n_1 - 1)P(n_1, n_2, t) \\ &- 4\kappa n_2(N_s - n_1 - n_2)P(n_1, n_2, t)\end{aligned} \tag{50}$$

Due to the added terms and complexity of eqs 49 and 50, we could not solve for them directly as we did for eq 17. Instead, they can be solved analytically as a system of linear differential equations, which limits the number of network strands N_s that can be described within an individual microregion. We leave the analysis of eq 50 for future work.

A.5. Equilibrated Distribution Models of Microregion Configuration

In some scenarios of network formation (particularly by step-growth polymerization), the probability distribution of different microregion configurations can be derived via combinatoric arguments, for example, in the case of reversible binding, when equilibrium is reached and the annealing process is complete (Table 2). We evaluate this limit here and find the probability distribution for a given microregion configuration $\{n_0, n_1, n_2\}$ with n_0 unbound s_0 strands, n_1 singly bound s_1 strands, and n_2 doubly bound s_2 strands, under the assumption that a total of m end-groups have bound. We do not consider how the pairs of end-groups are bound. For example, in the case of network strand binding to two branchpoints that are very far away from

Table 2. Overview of Different Approaches Used to Model End-Linked Networks for Both Chain and Step-Growth Polymerization Mechanisms

	Polymerization mechanism	
	Chain-growth	Step-growth
Model type	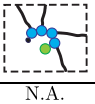	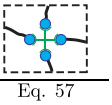
Equilibrated distribution	N.A.	Eq. 57
Master equation, quenched	Eq. 17	Eq. 49
Master equation, bond rearrangement	Eq. 28[a]	Eq. 50

[a] Bond rearrangement may not be realistic for chain-growth polymerizations.

https://dx.doi.org/10.1021/acs.macromol.0c01346
Macromolecules 2021, 54, 126−142

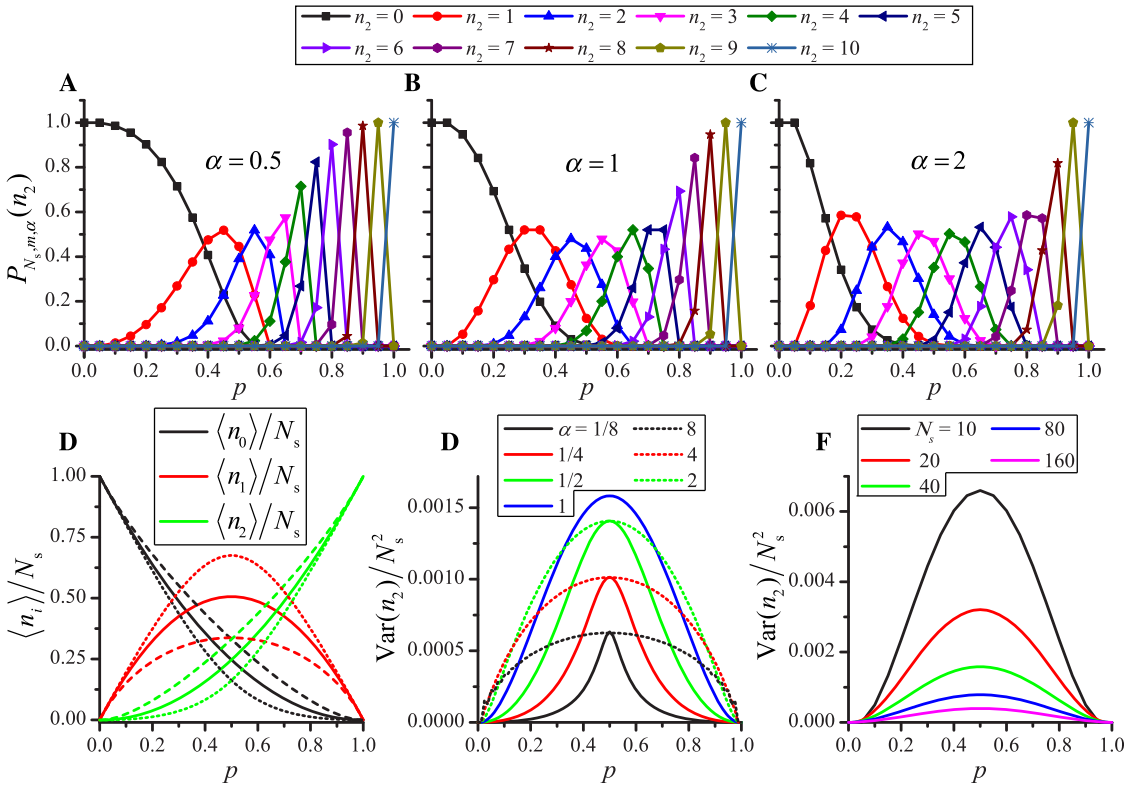

Figure 13. Results from the equilibrated distribution $P_{N_s,m,\alpha}(n_2)$, as evaluated from eq 57 for $N_s = 10$ and as a function of the extent of reaction $p = m/2N_s$ for (A) $\alpha = 0.5$, (B) $\alpha = 1$, and (C) $\alpha = 2$. Each point represents a different configuration $\{n_0, n_1, n_2\}$; those with the same n_2 are connected by lines. (D) Average populations $\langle n_i \rangle / N_s$ for $i = 0, 1, 2$, $N_s = 40$, and $\alpha = 0.5$ (dotted line), $\alpha = 1$ (solid line), and $\alpha = 2$ (dashed line). (E) Normalized variance of n_2/N_s as a function of p for $N_s = 40$ and several values of α. (F) Normalized variance of n_2/N_s for $\alpha = 1$ and several values of N_s. A maximum emerges at $p = 0.5$, whose value decreases with N_s. Notice the symmetry in $\langle n_1 \rangle$ and $\mathrm{Var}(n_2)/N_s^2$ about $p = 0.5$ for all values of α.

one another, we do not consider the restriction of certain states from existing by steric or other effects; instead, every binding site is accessible to every possible end-group, independent of spatial restrictions. We assume that each microregion examined is well mixed and that our assumptions follow mass-action kinetics.

At equilibrium, the time and order at which strands were linked do not affect configuration likelihoods, so the task of finding the probability distribution for $\{n_0, n_1, n_2\}$ is equivalent to finding the number of ways $N(n_0, n_1, n_2)$ one can distribute $\{n_0, n_1, n_2\}$ among N_s strands with m total bindings, where we assume equal probability between all potential conformations. The above quantities are related by $n_0 + n_1 + n_2 = N_s$ since all strands must be accounted for and by $n_1 + 2n_2 = m$ to include the contribution of each strand type to the total bound end-group count. Hence, a given microregion with configuration $\{n_0, n_1, n_2\}$ can be equivalently described by $\{N_s, m, n_2\}$. The extent of reaction p can also be determined from $\{N_s, m, n_2\}$ via $p = m/(2N_s)$. Combinatoric arguments yield $N(n_0, n_1, n_2)$ as

$$\mathcal{N}(n_0, n_1, n_2) = 2^{n_1} \binom{N_s}{n_0, n_1, n_2} \tag{51}$$

Here, the 2^{n_1} factor arises from the fact that the bound end-group on an s_1 strand can be arranged in two configurations per strand. The above can be rewritten using $n_0 = N_s - m + n_2$ and $n_1 = m - 2n_2$ as follows

$$\mathcal{N}(N_s, m, n_2) = \frac{2^{m-2n_2} N_s!}{(N_s - m + n_2)!(m - 2n_2)! n_2!} \tag{52}$$

Upon summing over n_2 with N_s, m fixed, we find $Z_{N_s,m}$, the partition function over all possible configurations, with N_s, m fixed

$$Z_{N_s,m} = \sum_{n_2=0}^{[m/2]} \mathcal{N}(N_s, m, n_2) \tag{53}$$

where $[\cdot]$ indicates the integer part of its argument. The equilibrium probability distribution can finally be calculated as

$$P_{N_s,m}(n_2) = \frac{\mathcal{N}(N_s, m, n_2)}{Z_{N_s,m}} \tag{54}$$

Equation 54 may be used to evaluate many different microregion properties, such as averages, variances, and higher moments. We begin with the average number of free, dangling, and intact strands, respectively, given by

$$\langle n_0 \rangle = N_s - m + \sum_{n_2=0}^{[m/2]} n_2 P_{N_s,m}(n_2) \tag{55a}$$

$$\langle n_1 \rangle = m - 2 \sum_{n_2=0}^{[m/2]} n_2 P_{N_s,m}(n_2) \tag{55b}$$

$$\langle n_2 \rangle = \sum_{n_2=0}^{[m/2]} n_2 P_{N_s,m}(n_2) \tag{55c}$$

https://dx.doi.org/10.1021/acs.macromol.0c01346
Macromolecules 2021, 54, 126−142

In eqs 55a−55c, the average, denoted by $\langle\cdot\rangle$, is taken across all microregions with the same N_s and m, or equivalently, using all possible configurations within a single microregion with N_s strands and m total number of bound end-groups. The above combinatoric argument assumes that end-group binding is accompanied by end-group annealing until equilibrium is reached, independent of the number of bound end-groups already present. However, within cooperative or uncooperative binding, bound end-groups may promote or hinder the binding of other end-groups. We include these phenomena by rewriting eq 52 as

$$\mathcal{N}(N_s, m, n_2, \alpha) = \frac{(2/\alpha)^{m-2n_2} N_s!}{(N_s - m + n_2)!(m - 2n_2)! n_2!} \quad (56)$$

where the reactivity parameter $\alpha > 1$ represents cooperative binding, penalizing dangling ends in favor of $s_1 \rightarrow s_2$ events. Values of $\alpha < 1$ represent uncooperative binding where $s_0 \rightarrow s_1$ events are favored. The neutral case is $\alpha = 1$. Finally, the equilibrium probability distribution $P_{N_s,m,\alpha}(n_2)$ can be written as

$$P_{N_s,m,\alpha}(n_2) = \frac{\mathcal{N}(N_s, m, n_2, \alpha)}{\sum_{n_2=0}^{[m/2]} \mathcal{N}(N_s, m, n_2, \alpha)} \quad (57)$$

We plot $P_{N_s,m,\alpha}(n_2)$ in eq 57 for several values of n_2, under three choices of α and as a function of the extent of reaction $p = m/(2N_s)$ in Figure 13A−C. The solid lines connect microregion configurations with the same n_2; we choose this representation as the number of intact "elastically effective" s_2 network strands is an important feature of polymer networks and determines both the mechanical modulus and swelling behavior of the network.[3] As α increases, all curves tend to shift to the left, as might be expected since increasing cooperative effects favor the emergence of s_2 strands for a given p. In Figure 13D, we plot the average strand fractions $\langle n_i\rangle/N_s$ for $i = 0, 1, 2$ as evaluated via eqs 55a−55c for $N_s = 40$ and as a function of p. Note that for all values of α, the average quantity $\langle n_1\rangle$ is a symmetric function of m about N_s as can be verified by imposing $m' = 2N_s - m$ in eq 55b and verifying that $\langle n_1\rangle$ remains unchanged. Since $p = m/2N_s$, this also implies that $\langle n_1\rangle$ will be symmetric about $p = 1/2$ for all values of α, as seen in Figure 13E,F. The $\langle n_i\rangle$ quantities in eqs 55a−55c closely match those obtained from eq 28 for all α, as can be seen upon comparing Figure 13D with Figure 9A−C. We also calculate the second moment $\langle n_2^2\rangle$ defined as

$$\langle n_2^2\rangle = \sum_{n_2=0}^{[m/2]} n_2^2 P_{N_s,m,\alpha}(n_2) \quad (58)$$

from which we obtain the variance $\mathrm{Var}(n_2) = \langle n_2^2\rangle - \langle n_2\rangle^2$ where $\langle n_2\rangle$ is derived in eq 55c. Similarly as for $\langle n_1\rangle$, one can verify that $\mathrm{Var}(n_2)$ is symmetric about $p = 1/2$ for all values of α. Since $n_1 = m - 2n_2$, $n_0 = N_s - m + n_2$, and given $\langle n_1\rangle$ and $\langle n_0\rangle$ from eqs 55a and 55b, $\mathrm{Var}(n_1) = \langle n_1^2\rangle - \langle n_1\rangle^2$ and $\mathrm{Var}(n_0) = \langle n_0^2\rangle - \langle n_0\rangle^2$ can also be derived using eqs 55c and 58. Figure 13E shows $\mathrm{Var}(n_2)/N_s^2$ as a function of p for different values of α. In each case, the maximum variance occurs when half of all possible end-groups have bound at $p = 1/2$. As α deviates from the neutral condition $\alpha = 1$, the bias toward certain bond types induced by cooperativity or uncooperativity causes the variance to decrease. In Figure 13F, we plot $\mathrm{Var}(n_2)/N_s^2$ as a function of p for different values of N_s: the curve remains symmetric about $p = 0.5$ and as N_s increases, the normalized variance decreases.

AUTHOR INFORMATION

Corresponding Author

Maria R. D'Orsogna − *Department of Mathematics, California State University, Northridge, Northridge, California 91330-8313, United States;* orcid.org/0000-0003-2828-9523; Email: dorsogna@csun.edu

Authors

Sam C. P. Norris − *Department of Bioengineering, University of California, Los Angeles, Los Angeles, California 90095-1600, United States;* orcid.org/0000-0003-4793-9085

Andrea M. Kasko − *Department of Bioengineering, University of California, Los Angeles, Los Angeles, California 90095-1600, United States;* orcid.org/0000-0003-2355-6258

Tom Chou − *Department of Biomathematics, University of California, Los Angeles, Los Angeles, California 90095-1766, United States; Department of Mathematics, University of California, Los Angeles, Los Angeles, California 0095-1555, United States*

Complete contact information is available at: https://pubs.acs.org/10.1021/acs.macromol.0c01346

Notes

The authors declare no competing financial interest.

ACKNOWLEDGMENTS

Funding for this work was provided by the National Institutes of Health through the NIH Director's New Innovator Award Program, 1-DP2-OD008533. S.C.P.N. gratefully acknowledges support from a Ruth L. Kirschstein Predoctoral Fellowship (NIH-F31DE026356). T.C. acknowledges support from the NSF through grant DMS-1814364. M.R.D. acknowledges support from the NSF through grant DMS-1814090. Both T.C. and M.R.D. also acknowledge support from the Army Research Office (W911NF-18-1-0345).

REFERENCES

(1) De Gennes, P.-G. *Scaling Concepts in Polymer Physics*; Cornell University Press, 1979.

(2) Flory, P. J. *Principles of Polymer Chemistry*; Cornell University Press, 1953.

(3) Rubinstein, M.; Colby, R. H. *Polymer Physics*; Oxford University Press: New York, 2003.

(4) Peppas, N. A.; Hilt, J. Z.; Khademhosseini, A.; Langer, R. Hydrogels in Biology and Medicine: From Molecular Principles to Bionanotechnology. *Adv. Mater.* **2006**, *18*, 1345−1360.

(5) Stauffer, D.; Coniglio, A.; Adam, M. Gelation and Critical Phenomena. *Polymer Networks*; Springer: Berlin, Heidelberg, 1982; pp 103−158.

(6) Sangeetha, N. M.; Maitra, U. Supramolecular gels: Functions and uses. *Chem. Soc. Rev.* **2005**, *34*, 821.

(7) Laftah, W. A.; Hashim, S.; Ibrahim, A. N. Polymer Hydrogels: A Review. *Polym.−Plast. Technol. Eng.* **2011**, *50*, 1475−1486.

(8) Nicolson, P. C.; Vogt, J. Soft contact lens polymers: an evolution. *Biomaterials* **2001**, *22*, 3273−3283.

(9) Hild, G. Model networks based on 'endlinking' processes: synthesis, structure and properties. *Prog. Polym. Sci.* **1998**, *23*, 1019−1149.

(10) Mark, J. E.; Sullivan, J. L. Model networks of end-linked polydimethylsiloxane chains. I. Comparisons between experimental and theoretical values of the elastic modulus and the equilibrium degree of swelling. *J. Chem. Phys.* **1977**, *66*, 1006−1011.

(11) Lin, C.-C.; Anseth, K. S. PEG Hydrogels for the Controlled Release of Biomolecules in Regenerative Medicine. *Pharm. Res.* **2009**, *26*, 631−643.

(12) Stanford, J. L.; Stepto, R. F. T.; Still, R. H. In *Chemical & Engineering News*; Labana, S. S.; Dickie, R. A., Eds.; American Chemical Society: Washington, D.C, 1984; Vol. *243*, pp 1−20.
(13) Mespouille, L.; Hedrick, J. L.; Dubois, P. Expanding the role of chemistry to produce new amphiphilic polymer (co)networks. *Soft Matter* **2009**, *5*, 4878.
(14) Buwalda, S. J.; Boere, K. W.; Dijkstra, P. J.; Feijen, J.; Vermonden, T.; Hennink, W. E. Hydrogels in a historical perspective: From simple networks to smart materials. *J. Controlled Release* **2014**, *190*, 254−273.
(15) Metters, A. T.; Bowman, C. N.; Anseth, K. S. A Statistical Kinetic Model for the Bulk Degradation of PLA- b -PEG- b -PLA Hydrogel Networks. *J. Phys. Chem. B* **2000**, *104*, 7043−7049.
(16) Tonelli, A. E.; Helfand, E. Elastically Ineffective Cross-Links in Rubbers. *Macromolecules* **1974**, *7*, 59−63.
(17) Gu, Y.; Zhao, J.; Johnson, J. A. A (Macro)Molecular-Level Understanding of Polymer Network Topology. *Trends Chem.* **2019**, *1*, 318−334.
(18) Seiffert, S. Origin of nanostructural inhomogeneity in polymer-network gels. *Polym. Chem.* **2017**, *8*, 4472−4487.
(19) Bastide, J.; Leibler, L. Large-scale heterogeneities in randomly cross-linked networks. *Macromolecules* **1988**, *21*, 2647−2649.
(20) Ikkai, F.; Shibayama, M. Inhomogeneity control in polymer gels. *J. Polym. Sci., Part B: Polym. Phys.* **2005**, *43*, 617−628.
(21) Bibbo, M. A.; Valles, E. M. Calculation of average properties of the pendant chains in a network. *Macromolecules* **1982**, *15*, 1293−1300.
(22) Dušek, K.; Dušková-Smrčková, M.; Fedderly, J. J.; Lee, G. F.; Lee, J. D.; Hartmann, B. Polyurethane networks with controlled architecture of dangling chains. *Macromol. Chem. Phys.* **2002**, *203*, 1936−1948.
(23) Stanford, J. L.; Stepto, R. F. T. Rate theory of irreversible linear random polymrisation. Part 1.—Basic theory. *J. Chem. Soc., Faraday Trans. 1* **1975**, *71*, 1292.
(24) Stanford, J. L.; Stepto, R. F. T.; Waywell, D. R. Rate theory of irreversible linear random polymerisation. Part 2.—Application to intramolecular reaction in A—A + B—B type polymerisations. *J. Chem. Soc., Faraday Trans. 1* **1975**, *71*, 1308.
(25) Ahmad, Z.; Stepto, R. F. T. Approximate theories of gelation. *Colloid Polym. Sci.* **1980**, *258*, 663−674.
(26) Schamboeck, V.; Iedema, P. D.; Kryven, I. Dynamic Networks that Drive the Process of Irreversible Step-Growth Polymerization. *Sci. Rep.* **2019**, *9*, No. 2276.
(27) Wang, R.; Alexander-Katz, A.; Johnson, J. A.; Olsen, B. D. Universal Cyclic Topology in Polymer Networks. *Phys. Rev. Lett.* **2016**, *116*, No. 188302.
(28) Lin, T.-S.; Wang, R.; Johnson, J. A.; Olsen, B. D. Topological Structure of Networks Formed from Symmetric Four-Arm Precursors. *Macromolecules* **2018**, *51*, 1224−1231.
(29) Kroll, D.; Croll, S. Heterogeneity in polymer networks formed by a single copolymerization reaction: II. Post-gelation structure and pendants. *Polymer* **2017**, *116*, 113−123.
(30) Kroll, D.; Croll, S. Influence of crosslinking functionality, temperature and conversion on heterogeneities in polymer networks. *Polymer* **2015**, *79*, 82−90.
(31) Balabanyan, A.; Kramarenko, E.; Ronova, I.; Khokhlov, A. Monte Carlo study of structure and kinetics of formation of end-linked polymer networks. *Polymer* **2005**, *46*, 4248−4257.
(32) Gilra, N.; Cohen, C.; Panagiotopoulos, A. Z. A Monte Carlo study of the structural properties of end-linked polymer networks. *J. Chem. Phys.* **2000**, *112*, 6910−6916.
(33) Leung, Y.; Eichinger, B. E. Computer simulation of end-linked elastomers. II. Bulk cured tetrafunctional networks. *J. Chem. Phys.* **1984**, *80*, 3885−3891.
(34) Leung, Y.; Eichinger, B. E. Computer simulation of end-linked elastomers. I. Trifunctional networks cured in the bulk. *J. Chem. Phys.* **1984**, *80*, 3877−3884.
(35) Hosono, N.; Masubuchi, Y.; Furukawa, H.; Watanabe, T. A molecular dynamics simulation study on polymer networks of end-linked flexible or rigid chains. *J. Chem. Phys.* **2007**, *127*, No. 164905.
(36) Chou, T.; D'Orsogna, M. R. Coarsening and accelerated equilibration in mass-conserving heterogeneous nucleation. *Phys. Rev. E* **2011**, *84*, No. 011608.
(37) D'Orsogna, M. R.; Lakatos, G.; Chou, T. Stochastic self-assembly of incommensurate clusters. *J. Chem. Phys.* **2012**, *136*, No. 084110.
(38) Yvinec, R.; D'Orsogna, M. R.; Chou, T. First passage times in homogeneous nucleation and self-assembly. *J. Chem. Phys.* **2012**, *137*, No. 244107.
(39) D'Orsogna, M. R.; Zhao, B.; Berenji, B.; Chou, T. Combinatoric analysis of heterogeneous stochastic self-assembly. *J. Chem. Phys.* **2013**, *139*, No. 121918.
(40) Davis, J. K.; Sindi, S. S. A mathematical model of the dynamics of prion aggregates with chaperone-mediated fragmentation. *J. Math. Biol.* **2016**, *72*, 1555−1578.
(41) Miller, D. R.; Macosko, C. W. A New Derivation of Post Gel Properties of Network Polymers. *Macromolecules* **1976**, *9*, 206−211.
(42) Macosko, C. W.; Miller, D. R. A New Derivation of Average Molecular Weights of Nonlinear Polymers. *Macromolecules* **1976**, *9*, 199−206.
(43) Tibbitt, M. W.; Kloxin, A. M.; Anseth, K. S. Modeling controlled photodegradation in optically thick hydrogels. *J. Polym. Sci., Part A: Polym. Chem.* **2013**, *51*, 1899−1911.
(44) Norris, S. C. P.; Chou, T.; Kasko, A. M. Diffusion of Photoabsorbing Degradation Byproducts in Photodegradable Polymer Networks. *Macromol. Theory Simul.* **2017**, *26*, No. 1700007.
(45) Flory, P. J. Molecular Size Distribution in Three Dimensional Polymers. III. Tetrafunctional Branching Units. *J. Am. Chem. Soc.* **1941**, *63*, 3096−3100.
(46) Webster, O. W. Living Polymerization Methods. *Science* **1991**, *251*, 887−893.
(47) Bowman, C. N.; Kloxin, C. J. Covalent Adaptable Networks: Reversible Bond Structures Incorporated in Polymer Networks. *Angew. Chem., Int. Ed.* **2012**, *51*, 4272−4274.
(48) Roberts, M. C.; Hanson, M. C.; Massey, A. P.; Karren, E. A.; Kiser, P. F. Dynamically Restructuring Hydrogel Networks Formed with Reversible Covalent Crosslinks. *Adv. Mater.* **2007**, *19*, 2503−2507.
(49) Yang, B.; Zhang, Y.; Zhang, X.; Tao, L.; Li, S.; Wei, Y. Facilely prepared inexpensive and biocompatible self-healing hydrogel: a new injectable cell therapy carrier. *Polym. Chem.* **2012**, *3*, 3235.
(50) Rodell, C. B.; Wade, R. J.; Purcell, B. P.; Dusaj, N. N.; Burdick, Ja. Selective Proteolytic Degradation of Guest−Host Assembled, Injectable Hyaluronic Acid Hydrogels. *ACS Biomater. Sci. Eng.* **2015**, *1*, 277−286.
(51) Tang, S.; Richardson, B. M.; Anseth, K. S. Dynamic covalent hydrogels as biomaterials to mimic the viscoelasticity of soft tissues. *Prog. Mater. Sci.* **2020**, No. 100738.
(52) Brown, T. E.; Marozas, I. A.; Anseth, K. S. Amplified Photodegradation of Cell-Laden Hydrogels via an Addition-Fragmentation Chain Transfer Reaction. *Adv. Mater.* **2017**, *29*, No. 1605001.
(53) Griffin, D. R.; Kasko, A. M. Photodegradable Macromers and Hydrogels for Live Cell Encapsulation and Release. *J. Am. Chem. Soc.* **2012**, *134*, 13103−13107.
(54) Yang, C.; DelRio, F. W.; Ma, H.; Killaars, A. R.; Basta, L. P.; Kyburz, K. A.; Anseth, K. S. Spatially patterned matrix elasticity directs stem cell fate. *Proc. Natl. Acad. Sci. U.S.A.* **2016**, *113*, E4439−E4445.
(55) Li, C.; Strachan, A. Free volume evolution in the process of epoxy curing and its effect on mechanical properties. *Polymer* **2016**, *97*, 456−464.
(56) Kloxin, A. M.; Kasko, A. M.; Salinas, C. N.; Anseth, K. S. Photodegradable Hydrogels for Dynamic Tuning of Physical and Chemical Properties. *Science* **2009**, *324*, 59−63.
(57) Wong, D. Y.; Griffin, D. R.; Reed, J.; Kasko, A. M. Photodegradable Hydrogels to Generate Positive and Negative Features over Multiple Length Scales. *Macromolecules* **2010**, *43*, 2824−2831.
(58) Kloxin, A. M.; Tibbitt, M. W.; Kasko, A. M.; Fairbairn, J. A.; Anseth, K. S. Tunable Hydrogels for External Manipulation of Cellular Microenvironments through Controlled Photodegradation. *Adv. Mater.* **2010**, *22*, 61−66.

https://dx.doi.org/10.1021/acs.macromol.0c01346
Macromolecules 2021, 54, 126−142

(59) Peng, K.; Tomatsu, I.; van den Broek, B.; Cui, C.; Korobko, A. V.; van Noort, J.; Meijer, A. H.; Spaink, H. P.; Kros, A. Dextran based photodegradable hydrogels formed via a Michael addition. *Soft Matter* **2011**, *7*, 4881.
(60) Zhu, C.; Bettinger, C. J. Light-Induced Disintegration of Robust Physically Cross-Linked Polymer Networks. *Macromol. Rapid Commun.* **2013**, *34*, 1446−1451.
(61) Tsang, K. M. C.; Annabi, N.; Ercole, F.; Zhou, K.; Karst, D. J.; Li, F.; Haynes, J. M.; Evans, R. A.; Thissen, H.; Khademhosseini, A.; Forsythe, J. S. Facile One-Step Micropatterning Using Photodegradable Gelatin Hydrogels for Improved Cardiomyocyte Organization and Alignment. *Adv. Funct. Mater.* **2015**, *25*, 977−986.
(62) Käpylä, E.; Delgado, S. M.; Kasko, A. M. Shape-Changing Photodegradable Hydrogels for Dynamic 3D Cell Culture. *ACS Appl. Mater. Interfaces* **2016**, *8*, 17885−17893.
(63) Arakawa, C. K.; Badeau, B. A.; Zheng, Y.; DeForest, C. A. Multicellular Vascularized Engineered Tissues through User-Programmable Biomaterial Photodegradation. *Adv. Mater.* **2017**, *29*, No. 1703156.
(64) LeValley, P. J.; Noren, B.; Kharkar, P. M.; Kloxin, A. M.; Gatlin, J. C.; Oakey, J. S. Fabrication of Functional Biomaterial Microstructures by in Situ Photopolymerization and Photodegradation. *ACS Biomater. Sci. Eng.* **2018**, *4*, 3078−3087.
(65) Norris, S. C. P.; Delgado, S. M.; Kasko, A. M. Mechanically robust photodegradable gelatin hydrogels for 3D cell culture and in situ mechanical modification. *Polym. Chem.* **2019**, *10*, 3180−3193.
(66) Norris, S. C. P.; Tseng, P.; Kasko, A. M. Direct Gradient Photolithography of Photodegradable Hydrogels with Patterned Stiffness Control with Submicrometer Resolution. *ACS Biomater. Sci. Eng.* **2016**, *2*, 1309−1318.

https://dx.doi.org/10.1021/acs.macromol.0c01346
Macromolecules 2021, 54, 126−142